DOE/NASA/0176-81/3
CR 165505

REFERENCE

SURVEY ON AGING ON ELECTRODES AND ELECTROCATALYSTS IN PHOSPHORIC ACID FUEL CELLS

TASK 10 OF CONTRACT DEN-3-176

Paul Stonehart and John Hochmuth

October 1981

PREPARED FOR:

NATIONAL AERONAUTICS AND SPACE ADMINISTRATION
Lewis Research Center
Under Contract DEN-3-176
Prepared Under Interagency Agreement DEAI-03-80ET17088

FOR:

U.S. DEPARTMENT OF ENERGY
Energy Technology
Division of Fossil Fuel Utilization

17 Cottage Road, Madison, Connecticut 06443
Telephone Area Code 203 245-7507

TABLE OF CONTENTS

ABSTRACT

This report discusses the processes which contribute to the decay in performance of electrodes used in phosphoric acid fuel cell systems. Loss of catalytic surface area, corrosion of the carbon support, electrode structure degradation, electrolyte degradation, and impurities in the reactant streams have been identified as the major areas for concern. There are no strategies available that are capable of predicting the long term effects of any of these processes based on the results of short term experiments.

The mechanism of sintering of platinum electrocatalysts in phosphoric acid is not clearly defined. Surface area loss with time can be correlated with a power law decay equation; however, the lack of understanding of the sintering process has severely limited progress in development of sintering retardant catalysts. The development of in situ electron microscopy techniques for the observation of sintering experiments is worthy of investigation.

The decline of electrode performance due to carbon corrosion and electrolyte degradation are minimal. The mechanism of carbon corrosion in phosphoric acid is understood and accelerated testing methods for screening of prospective electrocatalyst support materials have been developed. The interaction of carbon with platinum crystallites needs further study. Modification of the carbon surface appears to be a promising method for sintering retardation. Electrolyte degradation can be prevented by prudent electrolyte management schemes, although the effects of ammonia impurity are not yet completely understood.

In addition to ammonia, hydrogen sulphide is particularly deleterious to fuel cell electrode performance. The development of sulphur tolerant electrocatalysts probably will not have a large impact on fuel cell technology because of the susceptibility of steam reforming catalysts to sulphur poisoning and environmental restrictions.

Examination of the electrode structure could return the largest dividends. It is not clear that all the platinum in the electrode is utilized effectively. In fact, recent evidence suggests that significant improvement in platinum utilization can be obtained. Techniques need to be developed to measure the quantity of platinum which is available for reaction under fuel cell operating conditions. In situ ion specific adsorption measurements may be useful for

this purpose. A clearer understanding of the operation of porous gas diffusion electrodes is also required for optimization of electrode structures and assessment of the importance of various structure degradation modes. Transient experimental methods should contribute to this understanding.

I. INTRODUCTION

The acceptance of phosphoric acid fuel cells as a viable, economic method of generating electricity is critically dependent on the long term stability of the fuel cell system. Minimum lifetimes of 40,000 hr are required in order to compete with conventional generating methods. Since the generation of electricity by fuel cells occurs via electrochemical reactions, the stability of the electrodes is the most important factor in maintaining performance. The primary objective of this report is to review the extant fuel cell literature to determine those factors which contribute to the degradation of electrodes, hence, long term performance declines in phosphoric acid fuel cell systems.

The key component of the electrode is the electrocatalyst. Platinum supported on carbon is currently employed at both the anode and cathode in the phosphoric acid system. It is well known that supported catalysts generally exhibit activity declines with time. The loss of catalytic surface area, either by sintering processes or adsorption of impurities, results in a decrease in power density, and, therefore, a performance decline with time.

The corrosion of the carbon support by electrochemical oxidation also contributes to degradation of system performance. Corrosion of the carbon at the metal crystallite/support interface may weaken the interaction forces which bond the metal to the support, thereby enhancing the mobility of the platinum particles. Severe corrosion may result in loss of entire crystallites by dissolution in the electrolyte. The electrode structure may also be damaged to such an extent that electrical discontinuities are introduced.

Total elimination of surface area loss phenomena and carbon corrosion are not likely. Any improvement in surface area retention and corrosion properties of the electrocatalyst can be important, however, if substantial gains can be made in initial system performance. Examination of the operating characteristics of the porous gas diffusion electrode is essential to determine the utilization of the catalyst.

Electrolyte management is a serious concern for long term, stable operation of fuel cells. The electrical conductivity of the acid must be carefully controlled to ensure that dissolved ionic reactants are present at the active site and, thus, able to participate in the electrochemical reaction. If the cell matrix dries out, reactant gas crossover may occur, thereby decreasing the rate of reaction.

Recent advances in hydrocarbon steam reforming have widened the range of fuels from which hydrogen can be obtained. These fuels, however, are not particularly desirable since they contain a wide variety of impurities. How the fuel cell responds to these impurities determines the level of sophistication required for fuel cleanup so that performance may be maintained over long periods of operation.

Each of these topics is discussed in more detail in the following sections. Attention is focused on how the electrode is affected. Existing literature on long term stability testing is relatively sparse. The usual procedure is to measure the performance of pilot plant scale fuel cell stacks over a period of time. Design or operating characteristics are then modified based on the result of the test. With minor exception, there has been no attempt to develop predictive tools for estimating the long term effects of electrode decay modes on performance based on results of short term tests. Indeed, all previous long term performance models are strictly empirical in nature. The hazards of extrapolation using empirical models are great and well-documented. The only definitive approach for reliable model building is to obtain an understanding of the physical processes which are taking place. This is the approach taken in this review. Toward this end, the final section outlines those areas of research where substantial improvements in initial performance or maintenance of performance can be realized.

II. SURFACE AREA LOSS

Small metal particles in contact with one another tend to fuse at high temperatures. This coalescence phenomenon is called "sintering" by ceramists and metallurgists. Sintering can be used for practical benefit, for example, in many metal fabrication processes. Accompanying the fusion of the powder particles, however, is a concomitant loss of surface area. Since catalysis is a surface process, sintering is usually detrimental to the performance of metals used as catalysts. In order to maximize the effectiveness of solid catalysts, there has been a great incentive to prepare and maintain the metal as very small particles. The most desirable particle size is in the range 1-10 nm. Crystallites in this range have a large fraction of their atoms at the surface of the particle which, therefore, are available for catalysis. The relationship between dispersion (defined as the ratio of surface metal atoms to total metal atoms in the sample) and crystallite size assuming a cubic crystal with 0.25 nm lattice spacing is shown in Figure 1 (1). All metal atoms are surface atoms for cubic crystals with edge length less than 1 nm.

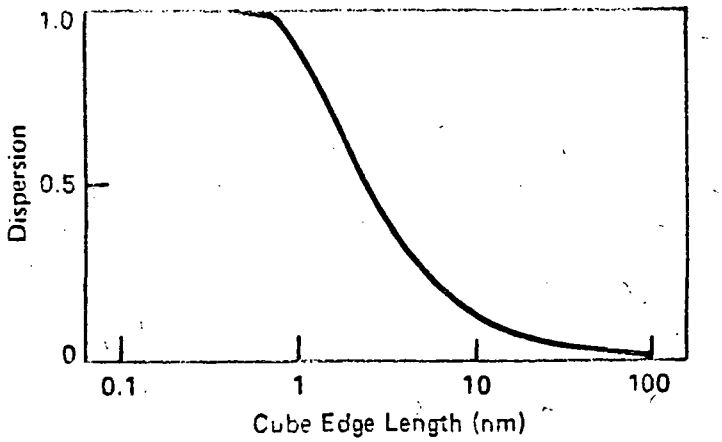

Figure 1. Dispersion vs. crystallite size for a hypothetical simple crystal.

Metal particles of less than 20 nm exhibit extremely low stability if the particles are allowed to touch one another. Platinum black, for example, with an initial particle diameter on the order of 20 nm, sinters at room temperature if exposed to oxygen and then to hydrogen (2,3). In the fuel cell environment, platinum black electrodes typically exhibit surface area declines of about 50% after only 200 hr in 96 w/o phosphoric acid at 150°C (4). Palladium black (7 nm crystallites) sinters in hydrogen at temperatures below 100°C (5).

The need for highly dispersed catalytic metals, combined with the impracticality of using metal powders, has led to the widespread use of porous, high surface area materials to support the small metal particles. High surface area ceramic materials such as alumina and silica are commonly used as carriers for gas phase applications. For operation in phosphoric acid fuel cells, the support must be conductive; therefore, the metal particles are usually deposited on carbon. The support markedly decreases the total amount of metal required to obtain a given level of catalytic activity. Platinum black has approximately 10-20 m^2 of platinum per gram, whereas supported platinum can exceed 200 m^2 of exposed platinum per gram of metal (6). Consequently, metal loadings can be dramatically reduced without loss of activity provided that diffusion of reactants to the metal does not limit the reaction rate. The use of supported catalysts in phosphoric acid fuel cells has resulted in a reduction of platinum metal loadings in the electrodes from 20 mg/cm^2 to 0.75 mg/cm^2 of active cell area (7). Although platinum particles are highly dispersed on the carbon support, there occurs, nevertheless, a considerable decrease in the platinum surface area with time due to platinum particle growth in the phosphoric acid environment at 100-200°C. Concurrent with the surface area loss is a decay in fuel cell performance.

The term "sintering" refers to the agglomeration of particles in physical contact. It should be emphasized, however, that this term is now accepted to describe the overall process whereby catalytic surface area is lost. It is quite clear that the catalytic activity <u>per unit weight of metal</u> will decrease with sintering because the fraction of surface atoms decreases. In most instances this is the result of metal particle growth, and it is the primary reason that sintering is of importance to catalyst users.

Several models have been proposed to explain the sintering behavior of supported catalysts. These models are based largely on the results of sintering in gas phase environments; however, they also apply to liquid environments (8,9,10). In the subsequent sections, these models are discussed in detail. Since the interaction of the metal with the support is important in determining the catalytic properties of supported catalysts (11), a section on metal-support interaction is included. The extant literature on sintering of supported platinum electrocatalysts in phosphoric acid environments is then reviewed.

Theoretical Models

The sintering of supported metal catalysts has become the subject of detailed fundamental investigation only in the last decade. Ruckenstein and Pulvermacher presented a mathematical treatment of sintering by metal crystallites in 1973 (12,13). Wynblatt and Gjostein (14,15) and Flynn and Wanke (16,17) used somewhat different approaches for describing this problem. Regardless of the basic assumptions made, the model must account for transport of metal across relatively large distances on the support and for incorporation of migrating metallic species into growing crystallites. Each of the three theoretical treatments cited above deals with these two components of sintering in its own way. The experimental data available to date favors no one model over the others.

The Ruckenstein-Pulvermacher analysis supposes that sintering occurs via migration, collision, and fusion of metal crystallites on the support surface, hence, it is commonly known as the crystallite migration model. This process is analogous to a two-dimensional Brownian motion of metal particles which undergo random collisions and subsequent coalescence. Either the migration or the coalescence step can be rate-determining. Rate expressions for particle growth were derived as extensions of the Smoluchowski coagulation theory (18). The general form of the rate expression for the change of catalytic surface area with time was shown to conform to the power law equation:

$$\frac{dS}{dt} = - KS^m \qquad (1)$$

where S is the surface area, K is a rate constant which depends on the metal loading, t is the sintering time, and m is an integer exponent which can vary between 2 and 8 depending on the nature of the rate controlling process. For

diffusion limited sintering, m was equal to 2 or 3, while for coalescence limited sintering, it was shown that $4 \leq m \leq 8$.

Sintering was treated as a two-dimensional evaporation-condensation process by Flynn and Wanke. The metal support system was pictured as seeking to establish an equilibrium between metal atoms on metal particles and those which have escaped to the support surface. This atomic migration model is similar to the model proposed by Ostwald (Ostwald ripening) for the change in mercury oxide particle sizes in solution (19). The migration of atoms across a support surface was first advanced by Shekhter (20) to account for the decrease in number and increase in size of globules of metal catalysts on filament supports. The model assumes that the rate at which atoms dissociate from metal particles is independent of particle size. The larger particles, therefore, grow at the expense of the smaller ones. The model also predicts that the size of the metal particles and the width of the distribution are critical parameters for determining the exponent m for fitting sintering data to Equation (1). Furthermore, the value of m is expected to vary during the course of a sintering experiment.

Wynblatt and Gjostein considered the events which occur on an atomic scale during sintering. The concepts of crystal nucleation and growth, particle migration and coalescence, and surface or vapor transport of metal were all discussed in terms of their relative importance in the overall rate of metal area loss. Order of magnitude rates for various steps in the proposed sintering sequence were calculated using data obtained on pure metals and supported metal films rather than on porous supported catalysts. As a result, the parameters were determined independently as opposed to determination by a fitting process.

On the basis of their calculations, Wynblatt and Gjostein concluded that particle growth occurred in either a "non-inhibited" or an "inhibited" mode. Both the crystallite migration and atomic migration models are examples of non-inhibited particle growth. The idea of inhibited growth arose from the observation of electron micrographs that platinum particles on flat alumina surfaces appeared to approach a limiting size during long term (about 70 hr) exposure at 700°C. This behavior was attributed to faceting of the metal crystallites. Crystallite growth, therefore, was inhibited by the requirement of a nucleation process for each new layer of atoms added to the particle. As a result, the rate constant in Eqn (1) depends on the crystallite size.

In addition to these models, several additional modes of sintering may contribute to the growth of metal particles on porous supports. The transport of metals through the vapor phase occurs when supported ruthenium catalysts are used in catalytic mufflers (21). If platinum is used as the catalyst, however, little loss of surface area is observed under the same operating conditions (22). Vapor phase transport in non-oxidizing environments is negligible for Group VIII metals (except ruthenium) at temperatures below 1000^{o}C; therefore, this mechanism may be due to volatilization of metal oxides (23). The liquid phase analogy to vapor transport is dissolution/redeposition. In this mechanism, small particles dissolve in solution by virtue of their greater surface energy. The dissolved metal diffuses along a concentration gradient and redeposits on larger crystallites. Bett, et al (8) have demonstrated that this crystallite growth mechanism is not likely to occur in hot phosphoric acid. This conclusion was based on the absence of a potential effect on the sintering rate coupled with thermodynamic considerations of the Pt/Pt^{2+} equilibrium. Platinum may enter solution, however, if corrosion of the carbon support occurs at the crystallite/support interface. The available liquid phase sintering literature suggests that crystallite growth probably does not occur in this manner. The remainder of this discussion, therefore, focuses on the crystallite migration, atomic migration, and the nucleation models.

Although these three theories represent three different views of sintering, they all agree on some points. First, they all predict that large crystallites grow at the expense of smaller ones. The pore structure will tend to stabilize the metal dispersion as will strong metal/support interactions. Finally, all the models can account for the increased stability of platinum in reducing atmospheres as opposed to oxidizing environments for a given set of parameters. It can be reasonably argued, however, that this latter correlation arises only after examination of experimental data.

The proposed models also disagree on a number of points. Experimental attempts to determine which mechanism predominates have not been conclusive. The major difference between the Ruckenstein-Pulvermacher and Flynn-Wanke models is the mode of transport. In the former model, metal crystallites are thought to migrate across the surface while for the latter, migration occurs by atoms or small metallic molecules. Ruckenstein and Pulvermacher argued that interactions between metal atoms and the support surface are too weak for dissociation to be energetically favorable (13).

They also pointed out that metal evaporation rates would be too slow to account for observed sintering rates. As an example, appreciable rates of sintering requires an activation energy for the escape of atoms from a large crystallite to be on the order of 80 kcal/mole. Since the heat of sublimation of platinum is 135 kcal/mole (24), the metal/support interaction energy must be at least 55 kcal/mole. Even though significant adhesion forces have been shown for oxide substrates (25), metal/support interactions are generally on the order of van der Waals forces (26).

Although direct evidence of crystallite migration is difficult to obtain, there are reports of this mode of particle growth in the literature. Bassett (27) observed translation of copper and silver islands on amorphous carbon and graphite at 252°C and Phillips, et al (28) inferred motion and coalescence of gold islands of up to 10 nm on silicon monoxide and amorphous carbon in the temperature range 227-427°C. Masson and co-workers (29,30) have shown that islands of both gold and aluminum in the range 2-5 nm can execute random walks on potassium chloride substrates at 70°C. Thomas and Walker (31) also report evidence for metal crystallite motion on carbon substrate.

The higher rate of sintering observed when presintered catalyst containing large platinum particles is added to the catalyst (32), on the other hand, suggests that large platinum particles accelerate agglomeration by acting as a sink for transported metal. To account for this observation, the transported metal must be highly mobile, since slowly diffusing crystallites would not be affected by large crystallites. The atomic diffusion model assumes rapid migration of metal atoms or molecules (16,17) similar to that observed in film growth studies (33).

The crystallite migration model of Ruckenstein and Pulvermacher describes a coalescence controlled condition in which the rate of merger of metal particles is the slow step in the sintering process. The Wynblatt-Gjostein analysis shows that, for metal crystallites smaller than about 5 nm, particle mobility is likely to account for sintering under reducing conditions; however, as the particle size increases, the crystallite surface diffusivity decreases sufficiently so that particle migration is unable to account for sintering of particles greater than about 7.5 nm (15). It was further shown that, on the basis of theoretical predictions, crystallite merger as the rate controlling step is generally not realizable under most sintering conditions.

The crystallite migration model also predicts that the particle size distribution as a function of time can be represented by a unique dimensionless distribution for the diffusion controlled case, as shown in Figure 2 (34).

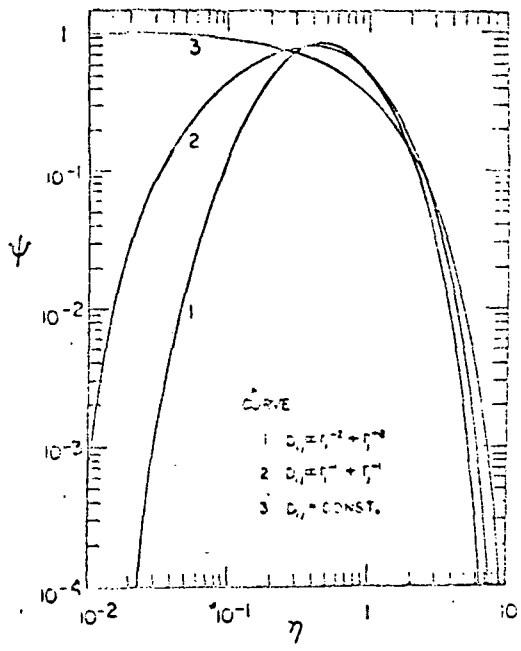

Figure 2. Similarity solution for diffusion controlled case.

This type of unique, dimensionless distribution function has been used by Swift and Friedlander for the mathematical description of coagulation processes (35). The experimentally observed bimodal particle size distributions obtained by sintering supported metal catalysts do not agree with this conclusion. The atomic migration model predicts a strong dependence of the rate of sintering on the metal to particle size distribution (11). Catalysts with broad or bimodal PSD are predicted to sinter more rapidly than catalysts with narrow PSD. Unisized particles would not sinter at all. The crystallite migration model does predict sintering for unisized distributions (13).

A final area for disagreement is the dependence of the sintering rate constant on metal loading. The crystallite migration model predicts a linear dependence on the metal loading (12,13). A number of investigators suggest that sintering by the atomic migration is independent of metal loading. This conclusion is only correct if the buildup of species in the transporting medium is small (11).

When the atomic migration model predicts a significant buildup of migrating atomic species, the surface loading becomes important. For this case, the rate of collision of migrating atoms with stationary metal crystallites depends on the surface concentration of migrating atoms, which in turn depends on the concentration of metal crystallites, i.e. the metal loading. For high metal loadings, the rate of capture is greater than for low metal loadings, hence the concentration of migrating metal atoms is lower.

In view of the complexity of supported metal sintering, it is clear that the mode by which supported metal crystallites grow is likely to depend on a number of factors including the nature of the metal and the support and the particular conditions under which the catalyst must operate. It is not surprising, therefore, that sintering data fitted to Eqn (1) give exponents ranging from 2 (36,27) to 13 (14). Flynn and Wanke, using data from the literature, show that the sintering order may change dramatically as sintering progresses (17). Results of several investigations are summarized in Table I.

TABLE I

Sintering Mechanism	Sintering Order	Ref.
Crystallite Migration	2-3 (Coalescence) 3-5 (Diffusion)	12 13
Crystallite Migration	7/2 (Diffusion)	28
Crystallite Migration	5-14	38
Atomic Migration	4 (Diffusion)	15
Atomic Migration	3	16,17
Atomic Migration	4-13	17

The available data on sintering kinetics are generally inadequate for confirmation of any particular mechanism. The best test for model discrimination is probably the ability to predict particle size distribution changes as a function of time, but such data are difficult to obtain experimentally as reflected by the different average radii obtained by different measurement techniques.

Metal Support Interactions

When small metal particles are deposited on high surface area materials, electronic interactions between the two materials may exist. Consider the case of a metal in contact with a semiconductor. If the work function of electrons in the metal is larger than the work function of electrons in the semiconductor, electrons will migrate from the semiconductor to the metal to establish an equilibrium state. The flow of electrons sets up a positive space charge in the semiconductor and a negative charge on the metal. The situation is reversed if the work function of the metal is less than that of the semiconductor. The Fermi level of a semiconductor can easily be altered by doping with different ions, thereby changing the electronic properties of the metal/semiconductor interface. Doping nickel oxide with lithium ions, for example, has been shown to affect the gas phase catalytic oxidation of carbon monoxide (39). The effect of different supports on the catalytic activity of supported metals has been reviewed by Geus (33) and by Solymosi (40).

Escard and co-workers (41,42) studied iridium catalysts deposited on a number of supports by x-ray photoelectron spectroscopy. A chemical shift in the iridium 4f doublet was observed. The magnitude of the shift depended on the nature of the support and was directly proportional to the Fermi level of the metallic oxides investigated.

Electron spin resonance spectroscopy of platinum supported on carbon indicated that platinum atoms donated electrons to the substrate (43,44). Sagert and Ponteau, however, later concluded from results of hydrogen-water-deuterium isotope exchange experiments that electrons were donated from the carbon to the platinum (45). Both platinum black and platinum supported on highly graphitized carbon black were examined.

The interaction between solid particles and substrates can also be examined by measurement of the forces of adhesion. Typically, adhesion energies less than 20 kcal/mole are observed (11). The atmosphere to which the catalyst is exposed markedly affects the adhesion of metal atoms to substrates. In general, cleavage of salt crystals in air gives faces with higher sticking probabilities for metal atoms than crystals cleaved in vacuum.

Bohme, et al (46) showed that the electrostatic force of adhesion was negligible compared to van der Waals forces for gold particles on silicon and gold substrates under vacuum conditions.

Pask and Fulrath (25) found greater adhesion between molten glass and gold, iron, and platinum metal surfaces when oxygen was present than under vacuum or reducing atmospheres. Geus (33) has reviewed the interactions between evaporated metal fibers and various support materials. The mobilities of silver and gold particles evaporated on silicon and on carbon were shown to be greater in water vapor than in vacuum. It was presumed that water molecules were able to penetrate between the metal particles and the substrate thereby reducing the interaction at the metal-support interface.

Bett, et al (8) report different degrees of surface area loss for platinum supported on graphitized carbon black for a number of liquid environments. There data are summarized in Table II. A number of additional investigations which demonstrate a reduction in the adhesion force in the presence of a liquid phase have been reviewed by Zimon (47).

TABLE II

Effect of Various Environments on the Surface Area Loss of Platinum on Carbon at 100°C

Environment	Pt on Carbon[a] surface area loss (%)		W_a (dyn/cm)
	20% Pt	5% Pt	
Ethylene glycol	11	—	2494
Bromobenzene	12	7	2516
96% H_3PO_4	22	28	2489
H_2O	14	16	2507
Toluene	15	18	2536
Hydrogen	0	0	2574

[a] In 24 hr.

Metal atoms adsorbed on substrates by vapor deposition have also been found to alter the electrical conductivity to a different extent than metal crystals, indicating electronic interaction between the metal and the support. The effect of the metal atoms was found to decay gradually, presumably due to the migration and incorporation of the atoms into metal crystals (48). The electrical resistivity of thin metal films has been observed to increase from the bulk metal resistivity when the film thickness becomes less than the electron mean free path length in the metal. The conduction of electrons in thin metallic films was discussed in detail by Anderson (49).

Adhesion of metal atoms during condensation onto substrates is also sensitive to the heterogeneity of the substrate surface. The well-known decorating effect, where nuclei concentrate around surface ledges or dislocations in film growth studies, is attributed to an increased metal atom interaction with these areas of the surface, and hence a higher metal atom population. The heterogeneous nature of most carbon substrates, therefore, might be used to advantage by providing sites of strong interaction with platinum resulting in a stable catalyst.

These studies indicate that the interaction of metal atoms and crystallites with typical substrates is extremely complex. Spectroscopic techniques, e.g. XPS and ESR, have been useful for characterizing supported catalysts. Extensive use of these techniques in future studies should lead to a clearer understanding of these interactions in electrocatalytic systems.

Surface Area Loss in Phosphoric Acid

The loss of platinum surface area with time has been recognized as a significant performance decay mode in phosphoric acid fuel cells. The early research in this area concentrated on identification of the mechanism of crystallite growth. More recently, attention has focused on methods of inhibiting migration of platinum through modification of the support.

Unsupported platinum black was shown by McKee (50) and Khassan, et al (51) to suffer significant surface area loss when heated in hydrogen at 100-200°C. The sintering rates of platinum black in 96 w/o phosphoric acid were found to be of comparable magnitude over the same temperature range (4,52) as indicated in Figure 3. When the data were fit to a power law rate, exponents considerably larger than would be predicted from the available theories were obtained. The

sintering of platinum black in phosphoric acid was also shown to depend on the potential (9). This potential dependence is shown in Figure 4.

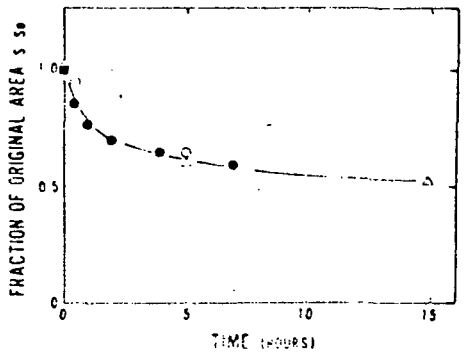

Figure 3. Sintering of Pt black at 150°C in hydrogen and in 96 wt% H_3PO_4. (△) Kinoshita et al (4), 96 wt% H_3PO_4, 0.5V; (○) Stonehart and Zucks (52), 96 wt% H_3PO_4, 0.5V; (●) McKee (50), hydrogen.

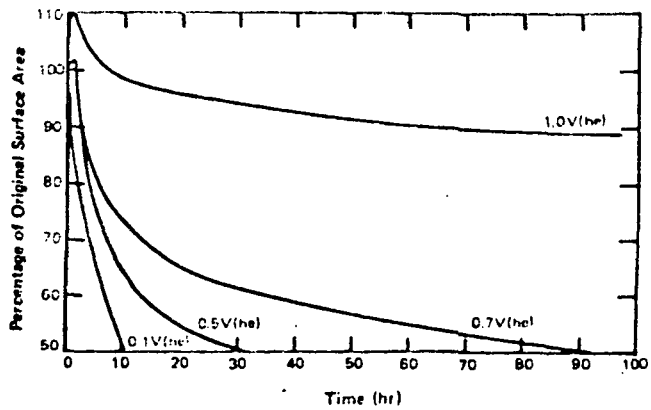

Figure 4. Effect of electrode potential on the loss of surface area of Pt black. 96 wt% H_3PO_4, 135°C, 24.5 m^2/gm Pt.

Connolly, et al (53) reported large decreases in the surface area of platinum crystallites dispersed on carbon in various electrolytes at 100-200°C. The surface area loss was not caused by dissolution of platinum since no platinum was found in solution and no loss of platinum from the catalyst was detected. The surface area loss was dependent on the initial crystallite size distribution, temperature, type of support, and the electrolyte. A detailed discussion of the mechanism by which platinum surface area was lost was not presented.

Tseung and Dhara (54) found that the area of platinum supported on graphite did not change when heated in air, whereas the platinum surface area decreased when used as a fuel cell electrode. Based on additional studies of platinum supported on antimony doped tin oxide in phosphoric acid, they concluded that the growth of platinum crystallites occurred by dissolution and redeposition of platinum ions. Other investigators (55,56), however, have found that platinum supported on graphite does sinter in gaseous environments suggesting a reinterpretation of the surface area loss mechanism.

Tseung also studied the effect of surface area loss on electrode performance (57). Electrodes fabricated from platinum black, platinum supported on antimony doped tin oxide, and platinum supported on carbon were sintered in air at 150°C for 720 hr. Initial and final performance was measured in 83 w/o phosphoric acid at 150°C. As indicated in Table III, only the platinum black electrode suffered a decrease in area coupled with loss in performance.

TABLE III

Effect of Heating on the Surface Area and Performance of Electrodes (150°C, Air)

Electrode	Initial Pt area M^2/g Pt	Final Pt area (after 720 hrs) M^2/g Pt	Initial Performance 83% H_3PO_4, 150°C mA/cm^2 at 600 mV	Final Performance 83% H_3PO_4, 150°C mA/cm^2 at 600 mV
10 mg Pt/cm^2	20.5	16.0	310	185
0.5 mg Pt on 10 mg Sb doped SnO_2/cm^2	21.0	20.4	50	50
2.1 mg Pt on 15 mg C/Cm^2	20.7	20.4	100	100

The electrodes were also held at 700 mV in 150°C phosphoric acid. All electrodes experienced a surface area loss under these conditions, as seen in Figure 5. The data were interpreted in terms of a dissolution/reprecipitation mechanism.

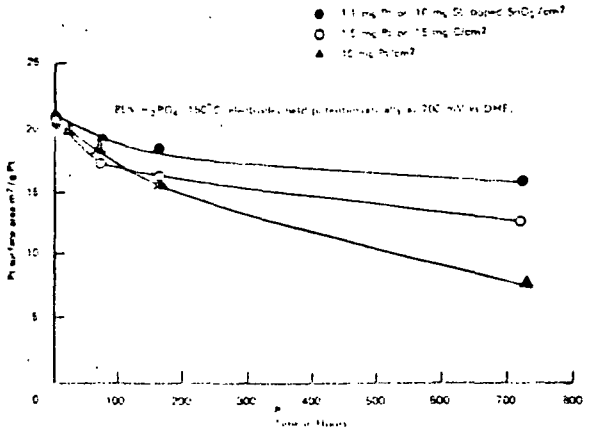

Figure 5. Change in Pt surface area with time.

Bett and co-workers (8) investigated the surface area loss of platinum on graphitized carbon black in phosphoric acid over the temperature range 100-200°C. Crystallite growth rates were apparently independent of the platinum content, shown in Figure 6, and only weakly dependent on potential, shown in Figure 7. The data were correlated using the integrated form of Eqn 1:

$$\frac{1}{S^n} = \frac{1}{S_o^n} + kt \qquad (2)$$

The order of the rate process was between 11 and 13, and the activation energy was estimated at 21 kcal/mole. The fit of Eqn 2 to the data, shown in Figure 8, was excellent. Because the rate did not appear to depend on metal loading, it was suggested that k was proportional to the platinum content, and the data, therefore, could be interpreted in terms of the atomic migration model.

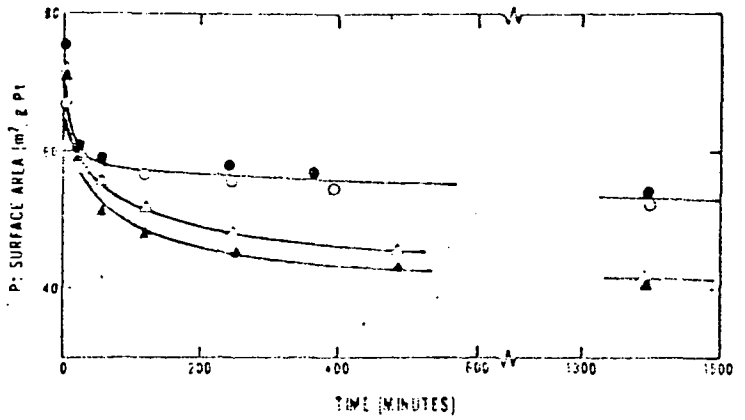

Figure 6. Effect of temperature and platinum metal content on crystallite growth of platinum on carbon in 96% H_3PO_4 at 0.8 V. (⊕) 5 wt% Pt, 100°C; (○) 20 wt% Pt, 100°C; (△) 5 wt% Pt, 160°C; (▲) 20 wt% Pt, 160°C.

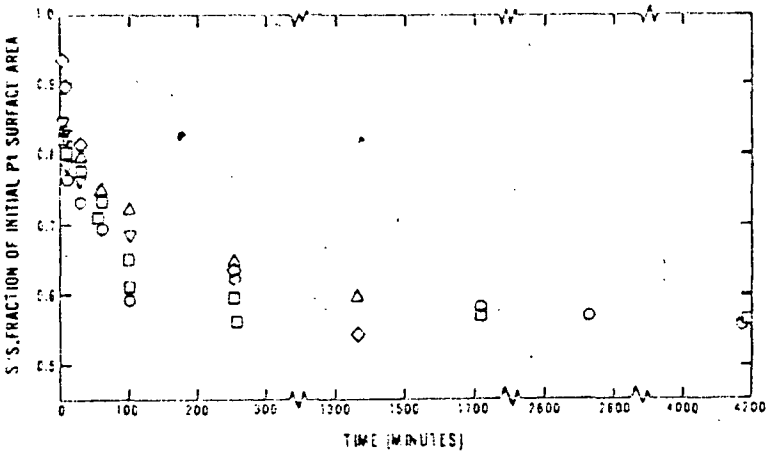

Figure 7. Influence of potential on Pt crystallite growth for 5% Pt on carbon in 96% H_3PO_4, 160°C. (○) 0.1 V; (□) 0.3 V; (△) 0.5 V; (◇) 0.8 V; (▽) 1.0 V.

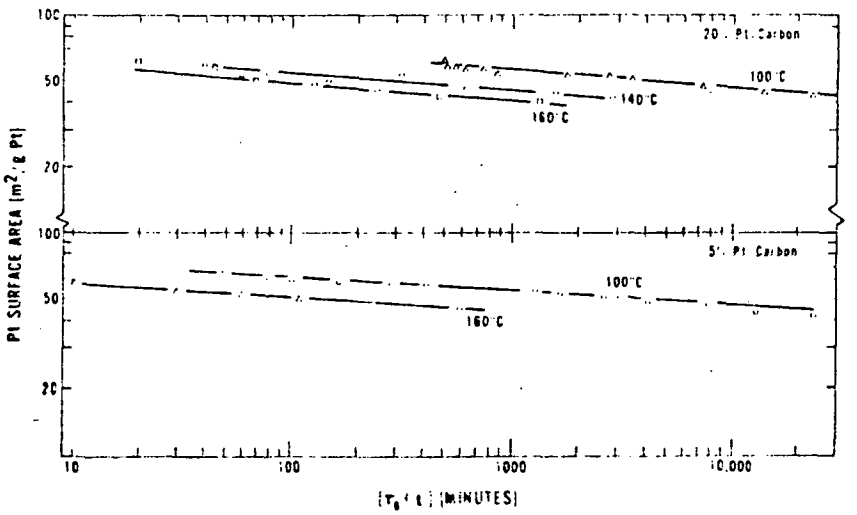

Figure 8. Plot of Eqn 2 for sintering of platinum on graphitized carbon black in 96% H_3PO_4, 0.8 V.

Stonehart and MacDonald (58) prepared electrodes from platinum dispersed on various carbon substrates. The carbons used were Vulcan XC-72R, Vulcan XC-72R heat treated to 2500°C for 2 hr under argon, Shawinigan acetylene black, and steam activated acetylene black. The electrodes were held at 700 mV in 165°C and 200°C phosphoric acid. The rates of surface area loss were found to depend on the carbon support; the highest rate of surface area loss was observed for the support exhibiting the highest corrosion rate. In addition, surface area loss was greater at the higher temperature for a given support. It was suggested that the higher corrosion rate at increased temperature might be a contributing factor to the decreased area of platinum. Substantial losses of platinum surface area were observed during the first hour of operation. The data were plotted to conform to Eqn 2. No values for n were reported and no discussion pertaining to the sintering mechanism was undertaken.

More recently, Gruver, et al studied the surface area loss of platinum supported on Vulcan XC-72 in a 191°C phosphoric acid fuel cell environment to define the sintering mechanism (59). A rapid initial surface area decline was also observed in this work. The data, shown in Figure 9, conformed to Eqn 2.

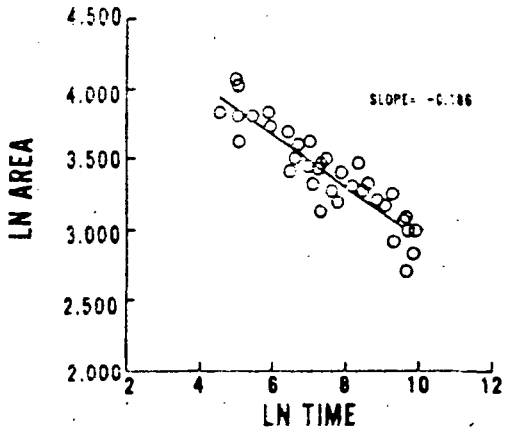

Figure 9. Plot of ln area as a function of ln t for Pt supported on Vulcan XC-72 at 191°C in H_3PO_4.

Transmission electron microscopy was used to examine both the platinum on carbon electrodes and platinum on carbon films at various sintering times. Examination of these micrographs led the authors to conclude that the primary mode of crystallite growth was by migration of platinum crystallites, although atom migration was not ruled out as a secondary contributing factor.

All of the previously cited investigations have focused on identification of the sintering mechanism. It is clear, however, that these studies have failed to define this mechanism unequivocally. Therefore, an alternative approach to the question of surface area loss in phosphoric acid fuel cell cathodes has been undertaken in recent years. This approach is to alter the properties of the support in some way in an effort to retard the growth of platinum crystallites on carbon.

Blurton, Kunz, and Rutt (60) employed an oxidation procedure to modify graphitized carbon black. Iron and copper salts were impregnated on the carbon, dried, and heated in nitrogen and then oxygen at the desired temperature. This treatment converted the iron and copper salts to the respective oxides which are known to catalyze the oxidation of graphite in a characteristic pattern (61). Iron oxide, for example, produces etch pits in the graphite basal plane (63). The resultant supports were then catalyzed with 5 w/o platinum by impregnation and thermal decomposition.

Comparison of surface area loss for catalysts prepared on the unoxidized and the iron oxide treated supports is shown in Figure 10.

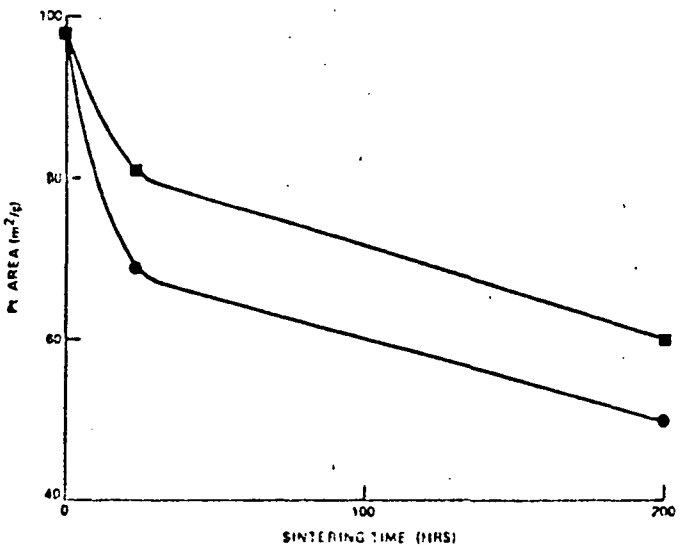

Figure 10. Area change of supported platinum tested in 102% H_3PO_4 at 190°C. (●) unoxidized graphite support; (■) support prepared by iron oxide (0.1% Fe) catalyzed oxidation of graphite to 15% weight loss.

Results are for 102 w/o phosphoric acid at 190°C. Quite clearly, the treated support improves the surface area retention. The copper oxide treated supports also improved surface area retention, but to a lesser degree than the iron oxide treated support. Platinum stability was independent of the iron concentration in the range 0.1-10 w/o Fe (see Figure 11) indicating that only a small fraction of the iron oxide particles were effective in forming the desired sites.

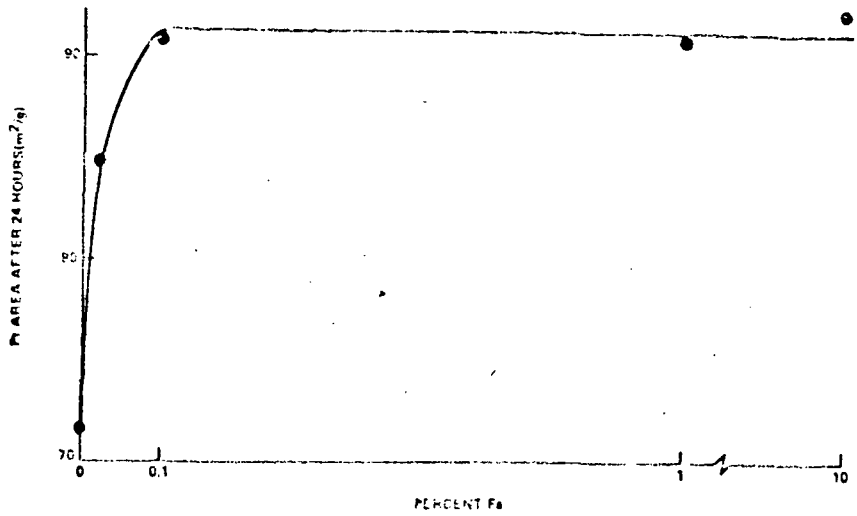

Figure 11. Effect of Fe concentration used for the support preparation on the Pt area after testing for 24 hr. Conditions: 98% H_3PO_4 at 160°C.

The superior surface area retention of the iron oxide treated support was attributed to the tendency to form etch pits during oxidation of the carbon as opposed to the channels formed by oxidation using copper oxide. Additional work on this approach using iron oxide and silver oxide to modify a wide variety of carbon materials has been undertaken (64).

Studies by Pan and Ciprios (65) showed that the sintering of supported platinum electrocatalysts in hot concentrated phosphoric acid was retarded when an activated charcoal (North American P-100) was used as the support material. It was proposed that the phosphorous present in the activated charcoal played a role in retarding platinum crystallite growth, possibly by interaction of phosphorous with platinum. Representative data are presented in Figure 12.

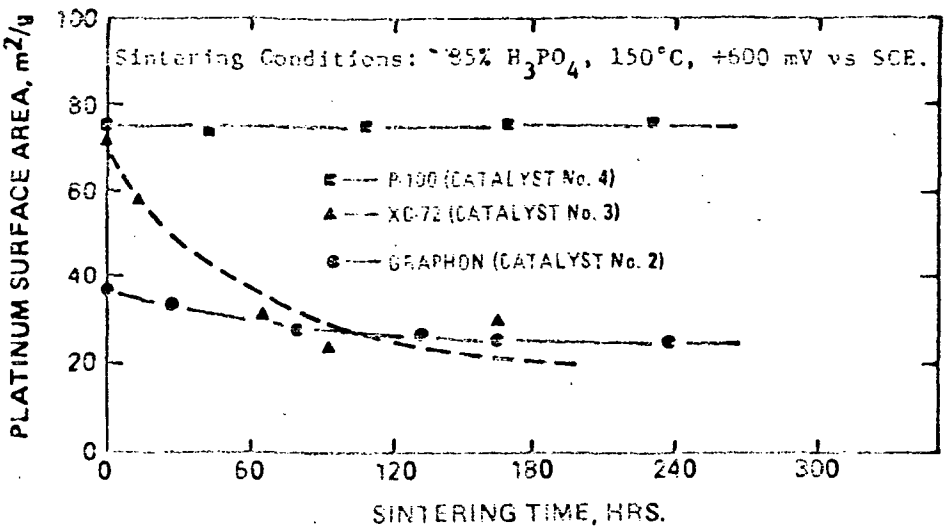

Figure 12. Comparison between ion-exchanged carbon-supported catalysts.

The electronic conductivity of P-100, however, was found to be low. Therefore, an additional study was undertaken to find a phosphorous addition treatment that would impart a stabilizing effect for platinum crystallites supported on other high surface area carbons (66). A vapor deposition technique and a thermal treatment with phosphoric acid were described for the addition of phosphorous to non-phosphorous containing carbons. Phosphorous deposited on carbons having no oxygen-containing surface groups was ineffective in retarding sintering. Phosphorous deposited on oxygenated supports provided some improvement in crystallite stability indicating that formation of stable phosphorous surface groups requires a substantial number of exchange sites.

The electrocatalyst pyropolymer structure and pore structure of Kocite* supports were modified by Welsh, et al (67) to investigate methods of improving electrocatalyst stability. Catalysts having a modified pore structure had structural stabilities comparable to standard Kocite supported catalysts. Those catalysts produced with modified pyropolymer structures exhibited a large spread of stability; however, platinum surface area retention on these supports were better than for the standard support electrocatalysts. It was concluded that varying the pyropolymer structure to give a more graphitized structure resulted in more stable performance than obtained with standard Kocite electrocatalysts.

* Registered Trademark, UOP.

III. CARBON CORROSION

Carbon blacks or heat treated carbon blacks are the only serious candidate materials for use as electrocatalyst supports for phosphoric acid fuel cells. The resistivity of carbon black may range from a few tenths to one ohm depending principally on the amount of oxygen containing surface groups on the black (68). Channel blacks with high surface oxygen coverage possess high electrical resistivity, whereas furnace blacks and acetylene blacks are low in surface oxygen and are very conductive. These latter materials, therefore, are highly desirable for fuel cell applications because only very slight ohmic losses are incurred. In addition, furnace blacks and acetylene blacks have moderately high surface areas facilitating the formation of small noble metal crystallites when conventional catalyzation procedures are used.

Carbon materials also possess undesirable physical characteristics. In particular, carbon is susceptible to electrochemical corrosion at certain fuel cell operating conditions. The corrosion mechanism is believed to occur by oxidation of the carbon. The degree of corrosion and the rate at which it proceeds are a function of the type of carbon, the electrode potential, the acid temperature, and the surface treatments given to the carbon.

The gas phase oxidation of carbon by oxygen has been extensively investigated. The primary oxidation products are carbon monoxide, carbon dioxide, and surface oxides. It has been pointed out by Thomas (69), however, that some uncertainty still exists as to the oxidation mechanism. It is believed that the formation of stable surface oxides inhibits the formation of CO and CO_2 since they decrease the active surface area. These oxides may in turn decompose at a rate slower than the oxidation processes to give additional gaseous products. The kinetics of the elementary reaction steps are dependent on temperature and the extent of carbon oxidation.

In contrast to gas phase oxidation of carbon, there is relatively little literature dealing with the electrochemical oxidation of carbon in aqueous media. Carbon is attacked by many oxidizing agents in aqueous suspension, e.g. permanganate (69,70), chromate (71), hypochlorite (71,72), persulphate (71,73), chlorine (69), and nitric acid (74,75). In the phosphoric acid fuel cell environment, the principal corrosion reaction is believed to be:

$$C + 2H_2O \rightarrow CO_2 + 4H^+ + 4e^- \qquad (3)$$

Surface oxides such as quinones, lactones, carboxylic acids, etc., are also formed.

Binder, et al (76) investigated the electrochemical corrosion of a number of carbons in sulphuric and phosphoric acids and in potassium hydroxide. The reaction products were observed to be carbon dioxide and surface oxides. The reaction rate was proportional to the carbon BET surface area. Janssen and Hoogland (77) postulated the formation of two carbon oxides for carbon electrodes in hydrochloric acid: a protective oxide which was reducible below -400 mV, and a surface oxide which formed on top of the stable oxide. The stable oxide could be decomposed at 1700 mV. Donnet and Ehrburger (78) examined the solution oxidation of furnace blacks by ozone in the absence of potential control. Two simultaneous oxidation mechanisms were postulated: the formation of carbon dioxide and the formation of partial oxidation products which remained as surface groups. Panzer and Elving (79) reviewed the nature of surface compounds on graphite electrodes prepared from pyrolytic graphite. Pyrolytic graphite oxidized preferentially on the graphite basal plane as opposed to edge planes.

Kinoshita and Bett (80) investigated the electrochemical oxidation of carbon black in 96 w/o phosphoric acid at 135°C. The total anodic current, the amount of CO_2 evolved, and the oxygen content of the carbon were all measured as a function of time and potential. Two anodic processes occurred: the formation of a surface oxide and the evolution of carbon dioxide. Both processes decreased with time, as shown in Figures 13 and 14. Carbon dioxide evolution eventually became the major reaction. The two processes were independent of each other since the surface oxide did not inhibit CO_2 formation. This can be seen in Figure 15. The surface oxide layer approached, but was less than, a theoretical monolayer, and continued to grow after carbon dioxide evolution became the primary process. Carbon corrosion was thought to occur by initial formation of surface carbon oxides followed by evolution of carbon dioxide. The corrosion rates were reported to be independent of water concentration and carbon dioxide partial pressure.

Since fuel cell operating temperatures have now approached 200°C, it is only in recent years that carbon corrosion at these conditions have been investigated (58,81). Stonehart and MacDonald (58) examined the effects of electrolyte temperature and concentration, operating potential, the type of carbon, and the nature of carbon surface treatments on the specific carbon corrosion rate.

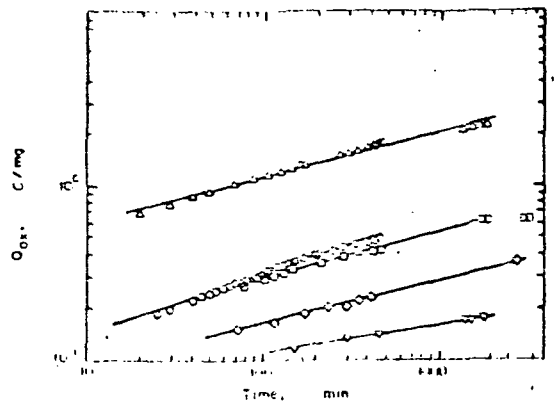

Figure 13. Growth of surface oxide on Neo Spectra carbon at various potentials in 96% H_3PO_4, 135°C. (△) 1000 mV (pre-reduced), (○) 1000 mV, (□) 900 mV, (◇) 800 mV, (▽) 700 mV.

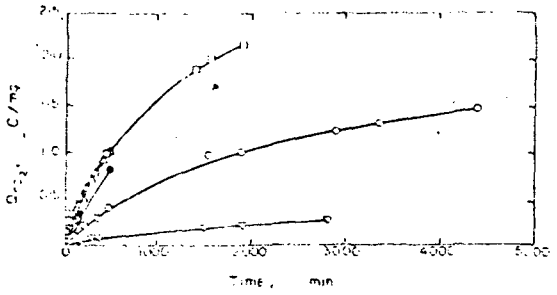

Figure 14. Evolution of CO_2 from Neo Spectra carbon at various potentials in 96% H_3PO_4, 135°C. (□) 1000 mV(pre-reduced at 0 mV for 24 hr), (●) 1000 mV (pre-reduced at 0 mV for 100 hr), (△) 1000 mV, (○) 900 mV, (▽) 800 mV.

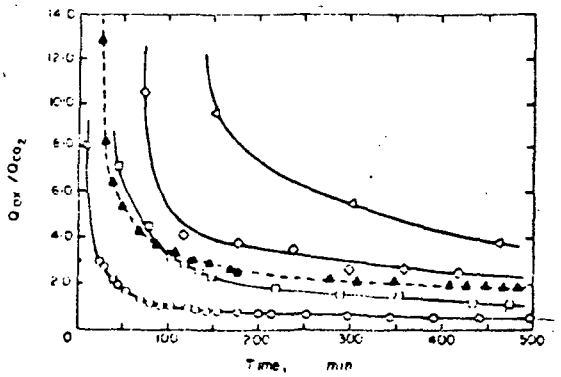

Figure 15. Q_{ox}/Q_{CO_2} as a function of time for Neo Spectra carbon at various potentials in 96% H_3PO_4, 135°C. (▲) 1000 mV (pre-reduced), (○) 1000 mV, (□) 900 mV, (◆) 800 mV, (◁) 700 mV.

At a given temperature, the corrosion currents increased with increasing potential. A similar relationship between corrosion current and temperature at a given potential was observed. Representative data are displayed in Figures 16 and 17.

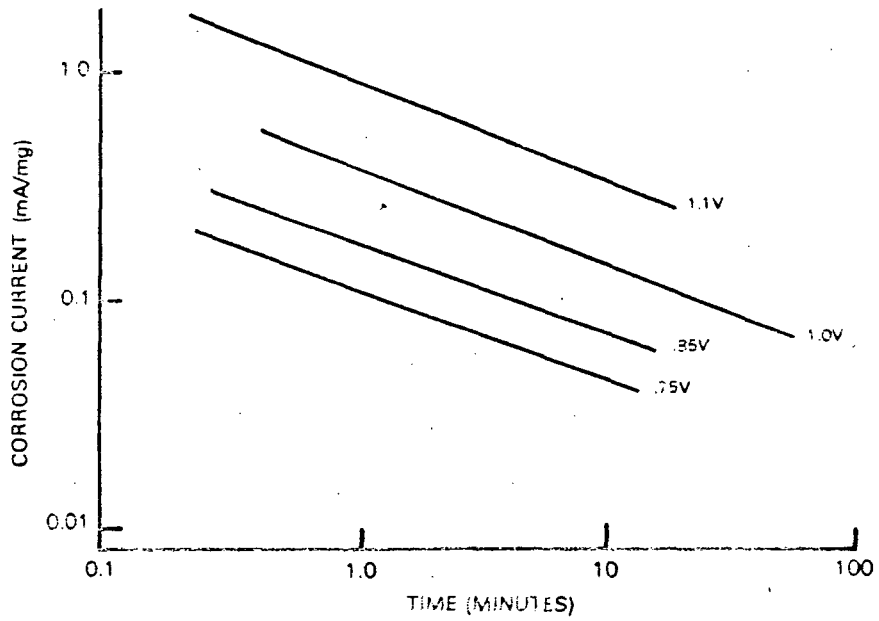

Figure 16. Vulcan XC-72R corrosion rates at 180°C over a range of potentials.

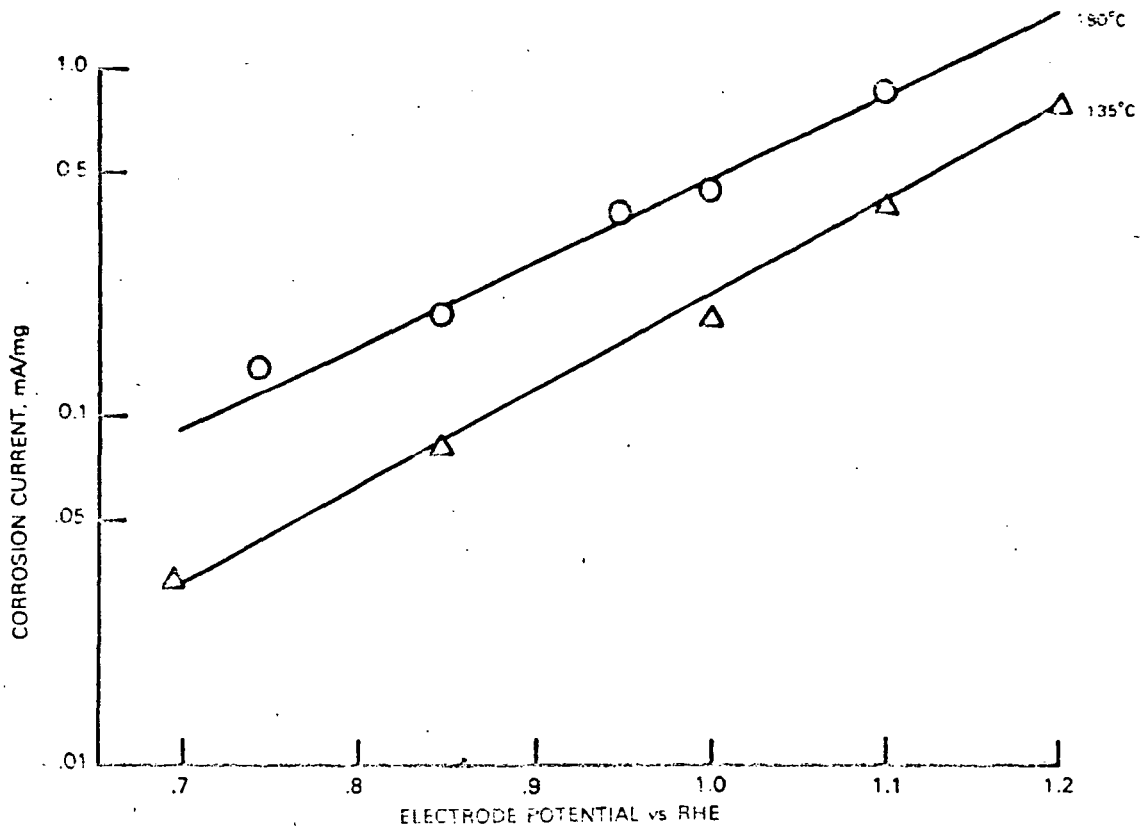

Figure 17. Vulcan XC-72R corrosion rates at one minute for different temperatures.

Corrosion rates varied greatly with the type of carbon; in general, the carbons with more highly ordered surfaces corroded at lower rates. Data for three of the carbon materials investigated are shown in Table IV.

TABLE IV

Specific Carbon Corrosion Rates at 1.0 V vs RHE and 210°C (mA/real cm^2 x 10^6)

Time (min)	Vulcan XC-72R	Shawinigan	XC-72R 2500HT
100	29	58	17
1000	4	28	8

The electrolyte structure and concentration were found to have a significant influence on the carbon corrosion rate. Arrhenius plots obtained in 106 and 103 w/o phosphoric acid exhibited the same apparent activation energies. The corrosion rates, however, were approximately five times greater for the lower acid concentration. Further experiments were conducted at lower acid concentrations where a lower apparent activation energy was observed. Data for Shawinigan acetylene black are shown in Figure 18. The change in Arrhenius slope occurred at the acid concentration where the phosphoric acid type changes from ortho to pyro.

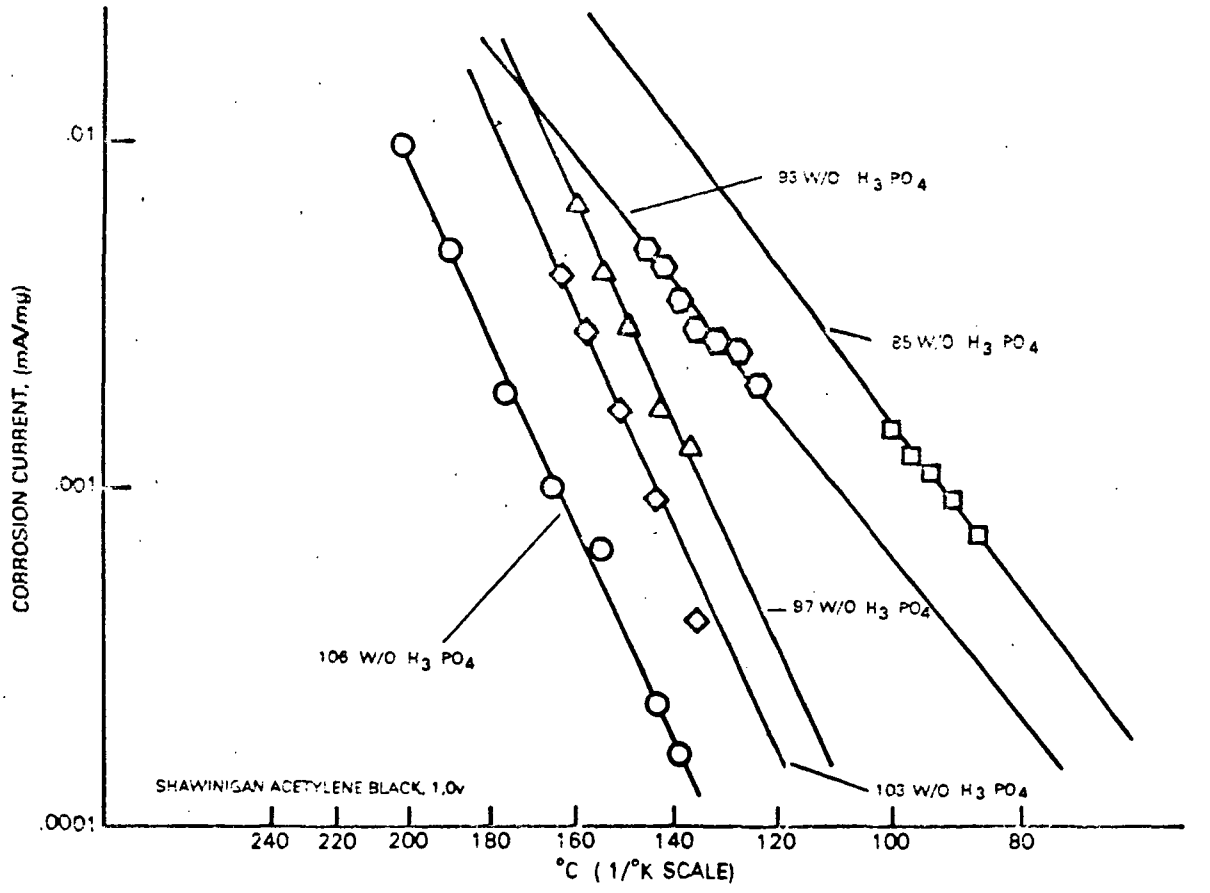

Figure 18. Arrhenius plots of the corrosion rates of Shawinigan acetylene black at 1.0 V in various H_3PO_4 concentrations.

The effect of heat treatment of the carbon was also found to depend on the structure of the parent carbon. The specific corrosion rates of Vulcan XC-72R subjected to various heat treatment temperatures in inert environments were independent of the heat treatment temperature. This relationship is demonstrated in Table V.

TABLE V

Effect of Heat Treating Vulcan XC-72R

Heat-treatment temperature, ^{o}C	BET SA, $m^2/g.$	Tafel slope range, mV	Tafel slope at 1000 min, mV	Specific corrosion rate @ 1000 min., $mA/real\ cm^2 \times 10^6$
As-received	254	150-190	190	4.6
800	211	150-180	-	4.7
1200	160	125-140	120	6.25
1400	141	110-120	115	5.3
1800	95	110-120	110	4.4
2500	65	100-110	100	2.6

$180^{o}C$ and 1.0V vs RHE

Heat treatment did alter the graphitic layer spacing in a systematic manner, however. In addition, the corrosion Tafel slope decreased with increasing heat treatment temperature. The relationship between measured Tafel slope and graphitic layer spacing, shown in Figure 19, was linear. Little difference in either Tafel slope or specific corrosion rate at 1 V was observed for similar experiments using Shawinigan acetylene black. It was concluded that the Tafel slope was indicative of the degree of disorder of the carbon surface.

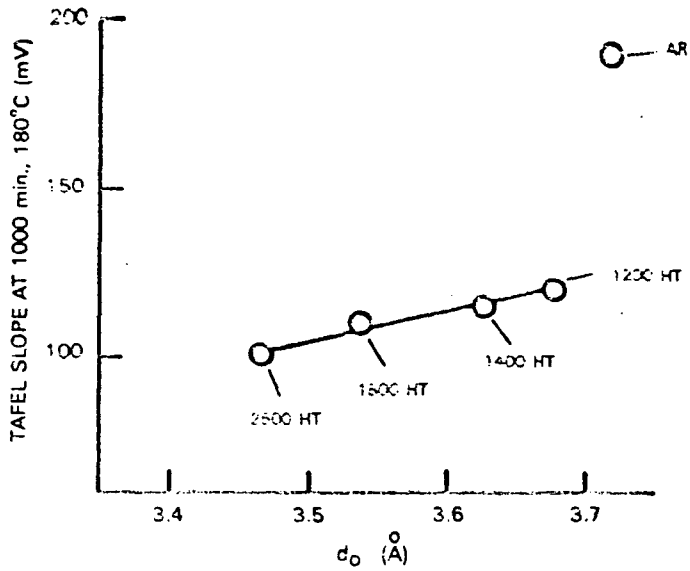

Figure 19. Tafel slopes vs d_o for heat-treated Vulcans.

IV. ELECTRODE STRUCTURE

The desired attributes of phosphoric acid fuel cell electrodes are high performance, long life, and low cost. Although high performance is directly related to the intrinsic activity of the catalyst, the electrode structure also plays a significant role as it is the nature of the structure that provides the gas-liquid-solid interface required for reaction to occur.

There are three distinct porous electrode systems. In the first system, a porous electrode is immersed in an electrolyte containing dissolved fuel or oxidant, so that the electrolyte and dissolved reactants flood the interior of the structure. High concentrations of methanol dissolved in alkaline electrolyte can be oxidized using this type of electrode. The advantage of using a porous electrode as opposed to a solid electrode is clear; some of the internal area of the porous structure will promote the electrochemical reaction.

The second type of porous electrode system is the flow-through electrode system. In this system, fuel or oxidant is dissolved in the electrolyte which is then forced through the porous electrode. The internal area of the electrode is again used to advantage; however, the electrode pore structure may be important for efficient electrode operation. The chlorine electrode used in zinc-chlorine batteries is a flow-through type electrode.

The third porous electrode system is the gas diffusion electrode. Here, a gaseous reactant is diffused through a hydrophobic phase to the reacting surface of an electrocatalyst which is wetted by electrolyte. This type of porous electrode system is employed in phosphoric acid fuel cells.

Operation of Gas Diffusion Electrodes

One of the major theoretical problems associated with the use of porous gas diffusion electrodes in fuel cells is an understanding of the mode of operation of the electrode. Any mathematical model which describes electrode operation must include a mechanism by which gaseous reactant arrives at a catalytic site on the electrode where it can react electrochemically. A sound understanding of this overall process will aid in defining the optimum performance for a particular electrochemical reaction. Any physical model of how gas diffusion electrodes work should be capable of explaining how the limiting current depends on the electrode structure, the degree of electrolyte penetration, the

reactant concentration, and the electrolyte resistance. The model must also be consistent with experimental performance curves. This, of course, presumes knowledge of the electrokinetic parameters of the reaction under study. Most practical gas diffusion systems are extremely complex in structure. It is highly unlikely that any simple model will be capable of accurately predicting the electrode behavior. Researchers in this area, therefore, have attempted only to investigate whether models can predict the general behavior of porous gas diffusion electrodes.

The solubility of oxygen in phosphoric acid is on the order of 10^{-6} g moles/cm^3 (82). Diffusion coefficients for the same system over a broad range of temperatures and acid concentrations have been measured and are of the order of 10^{-5} cm^2/sec (83). Extensive experimental work on the performance of gas diffusion electrodes have shown that electrodes which are flooded with electrolyte are not capable of supporting much current, and it is generally accepted that a three-phase boundary is necessary to obtain current densities on the order of 100-1000 ma/cm^2. Understanding how the three-phase boundary operates, therefore, is of paramount importance.

Justi and Winsel (83) described the possibility of gas adsorbing on bare metal followed by transfer by surface diffusion across the metal surface. The adsorbed species eventually cross a gas-liquid-metal boundary and react electrochemically. Since gases adsorb very rapidly on bare metal surfaces, it would be expected that only small amounts of metal exposed to the gas would be required. Experimental work, however, has shown that significant quantities of exposed metal are required for maximum current (85,86).

Another mode of operation is that the gas must first dissolve in the electrolyte and diffuse to the electrocatalyst surface. Two situations are shown in Figure 20. The diffusion path length at the three-phase boundary is very small; therefore, such a model would predict that the electrode could support considerable current. This model is referred to as the simple-pore model.

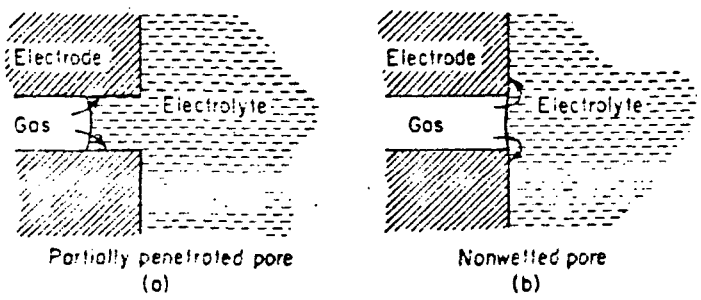

Figure 20. Simple-pore model.

Will found that when a thin platinum wire was partially submerged in an electrolyte, the electrolyte spread up the wire to a considerable distance beyond the edge of the bulk meniscus (85). He postulated that a similar electrolyte film would coat the interior surface of the pores within a porous electrode structure. This thin film model is illustrated in Figure 21. Evidence for the existence of thin films in porous electrodes has been reported by Austin, et al (87) but it is difficult to rationalize thin films at non-wetting electrodes unless it is assumed that micropores will wet due to capillary action but the bulk surface will not.

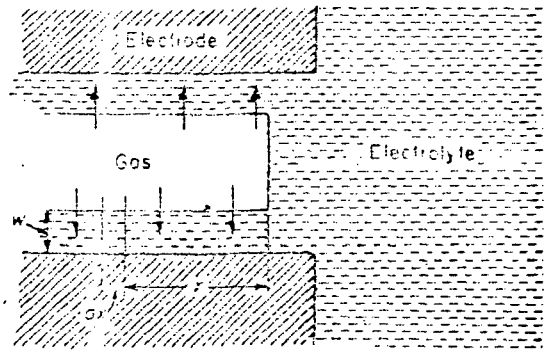

Figure 21. Thin-film model.

The majority of porous gas diffusion electrodes involve a multiple scale of porosity. The pore size distribution is generally characterized by two widely separated ranges. This porosity is the result of forming the electrode from a fine powder, e.g. carbon, which is itself porous. Grens II developed a dual scale porosity model in which the larger pores are filled with reactant gas and smaller pores are flooded with electrolyte by capillarity (88). A highly idealized representation of the model is illustrated in Figure 22.

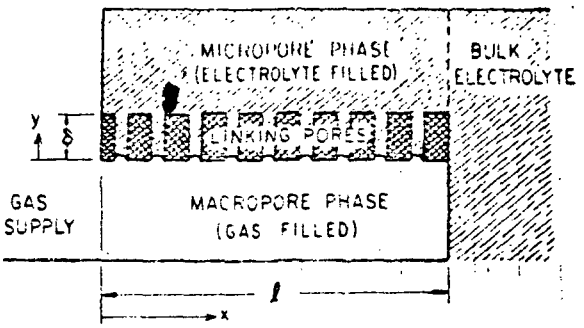

Figure 22. Model for gas electrode with double scale of porosity.

Horowitz (90) and Giner and Hunter (89) also consider bonded porous gas diffusion electrode structures exhibiting a dual scale of porosity. The working mechanism of the structure is explained by assuming that the catalyst particles form porous agglomerates which are flooded with electrolyte under operating conditions. The catalyst agglomerates are held together by a hydrophobic phase which provides channels for the gaseous reactant. Reactant gas diffuses through these channels, dissolves in the electrolyte, and, after diffusing a short distance in the filled agglomerate pores, reacts on available sites of catalyst particles. A schematic representation of this flooded agglomerate model is shown in Figure 23.

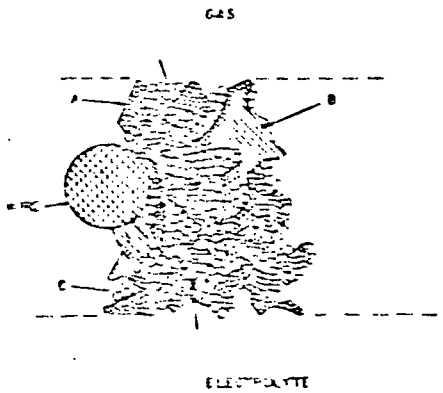

Figure 23. Schematic representation of a hydrophobic, porous electrode model of Teflon-bonded platinum black. A. Catalyst particle; B. Agglomerate; C. Teflon particle.

In general, all the models result in differential mass balances which are mathematically intractable and, therefore, require numerical solutions. The most common approach, however, has been to simplify the equations so that analytical solutions can be derived. The characteristics of each of these models is discussed in more detail in the following sections.

1. Simple Pore Model

The simple pore model description of porous gas diffusion electrodes was introduced by Austin, et al (87). The effects of the kinetic and physical parameters on the current density-overpotential and current distribution relations were not clearly addressed. These problems were considered in more detail by Srinivasan and co-workers (91). The structure of actual porous electrodes was considered to be too complex, so the mathematical treatment was simplified by assuming that the pores were uniform, parallel, and cylindrical. An average pore diameter was

assumed. Further simplifying assumptions were employed to permit analytical solutions; however, numerical solutions of the resulting differential mass balances were also performed.

On the basis of both the theoretical analysis and the numerical calculations, it was shown that gas diffusion through the electrolyte-free part of the pore structure was always very fast for pore radii greater than 10^{-4} cm compared to the rates of processes which occur in the electrolyte part of the pore. Below pore radii of 10^{-4} cm, gas diffusion was predicted to affect the reaction rate at high current densities.

Dissolution of reactant gas at the gas-electrolyte interface was shown to be fast under all conditions and thus would cause no problems. The limiting current density due to gas dissolution was estimated at about $10^5 A/cm^2$.

A two-dimensional treatment for processes taking place in the electrolyte occupied part of the pore was not possible for all forms of polarization. A one-dimensional treatment was used, however, for current densities lower than the limiting current by at least a factor of 4. Using this treatment, the ohmic potential was shown to be small up to the limiting current, thereby reducing the problem to one of activation and concentration polarization. Numerical solutions for all forms of polarization for parameters reflecting the operation of a platinum black electrode were also carried out. The current density distribution in a pore and the current density-overpotential relations are shown in Figures 24 and 25.

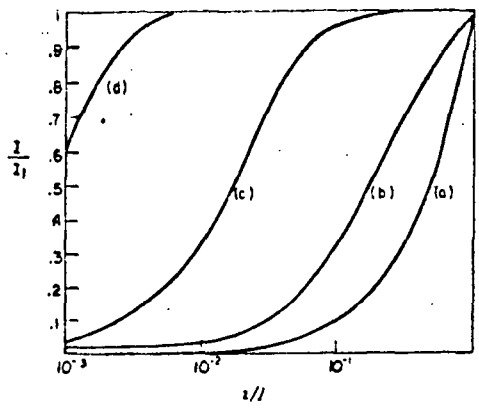

Figure 24. Current distribution relations for case where all forms of polarization are considered. Values of $DnFc^o$ and κ as in Figure 25. (a) Uniform current distribution in the pore, e.g., with $i_o = 10^{-12}$ A cm^{-2} and $\eta = 0.1$ V; (b) $i_o = 10^{-9}$ A cm^{-2} and $\eta = 0.1$ V; (c) $i_o = 10^{-12}$ A cm^{-2} and $\eta = 0.65$ V; (d) $i_o = 10^{-9}$ A cm^{-2} and $\eta = 0.65$ V.

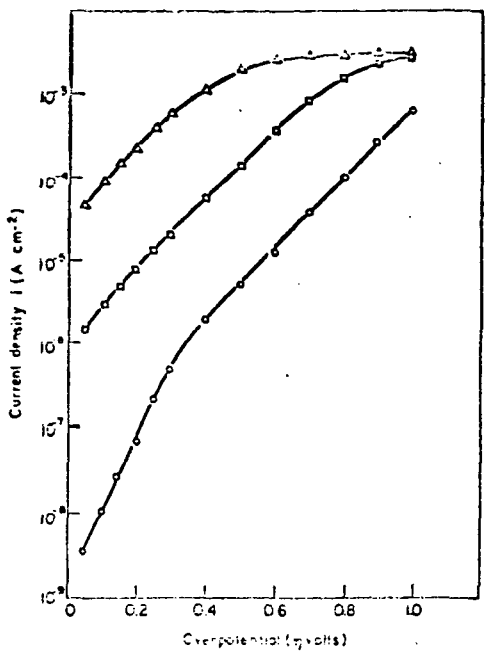

Figure 25. Overpotential current density relation for case where all forms of polarization are considered. Assumed parameters: $DnFc^{o}$ - 10^{-7} A cm^{-1}, κ = 1 Ω^{-1} cm^{-1}; ○, i_o = 10^{-12} A cm^{-2}; □, 10^{-9} A cm^{-2}; △, 10^{-6} A cm^{-2}.

The case of activation and concentration polarization was analyzed in both one and two dimensions. The limiting current density varied inversely with the pore diameter. Small pores on the electrolyte side and large pores on the gas side, therefore, are most desirable. This type of design had previously been considered only from the point of view of meniscus stability, although Swinkels had demonstrated the necessity of such a structure from kinetic considerations (92).

In the presence of concentration polarization, the simple pore model predicts that most of the current is generated over a short pore length for reasonable current densities. This conclusion suggests that platinum crystallites supported on carbon should be preferentially located near the electrocatalyst support pore mouth.

The model also predicted considerable increase in attainable current density, i.e. 2 to 3 orders of magnitude, on elimination of concentration polarization. Furthermore, the presence of ohmic polarization shifted the region of activity towards the bulk electrolyte end of the pore.

2. Thin Film Model

The existence of thin films on porous substrates was demonstrated by Austin, et al (87) using a fritted glass filter disc placed in a shallow layer of densely covered liquid. The liquid rapidly filled the frit by capillary action. Although the pore size distribution of a glass frit is large, it is reasonable that the fine pore system of a wetted fuel cell electrode will behave in a similar manner. If it is assumed that the film is long compared to its thickness, the mass transfer and kinetic processes can be considered to be one-dimensional along the film. Knowing the form of the electrochemical kinetic equations, it is possible to derive analytical equations relating current density to polarization for certain limiting cases.

Will (85) and Austin (93) considered the case where the electrochemical reaction was fast, dissolved gas diffused across the thin film to a reaction site, and ions traveled along the film to the same reaction site. It was assumed in these treatments that the only concentration gradient was that of the dissolved gas. Austin also considered the case of rapid gas diffusion across the film, slow reaction, and ohmic effects in the film.

Srinivasan and Hurwitz considered the case where all forms of polarization are present (94). Analytical expressions could not be derived for this situation. Numerical solutions were obtained for a number of combinations of electrode parameters. The limiting current density could be increased by decreasing the film thickness, increasing the diffusivity and/or solubility of the gaseous reactant in the electrolyte, or increasing the electrolyte conductance. These relationships are demonstrated in Figures 26-28.

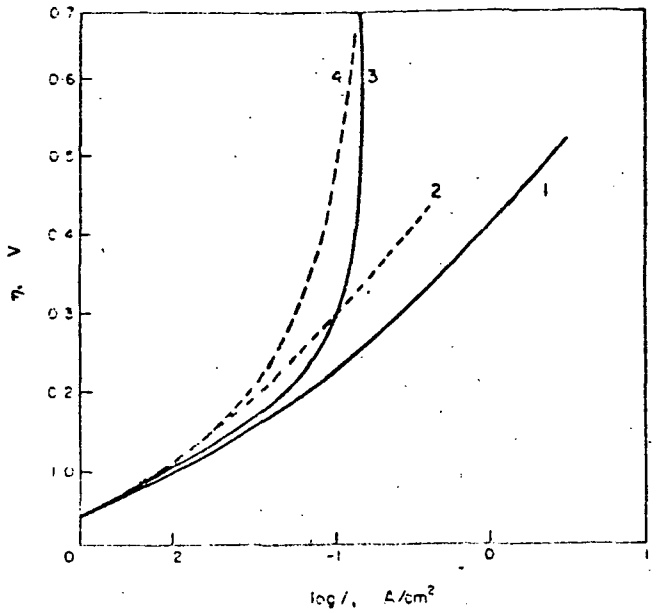

Figure 26. Current density/overpotential relationship for case where all forms of polarization are taken into account, showing effect of variation of κ or product $DmFc^{o}$. 1) $\kappa = 1$, $DmFc^{o} = 10^{-4}$; 2) $\kappa = 0.1$, $DmFc^{o} = 10^{-4}$; 3) $\kappa = 1$, $DmFc^{o} = 10^{-9}$; 4) $\kappa = 0.1$, $DmFc^{o} = 10^{-9}$.

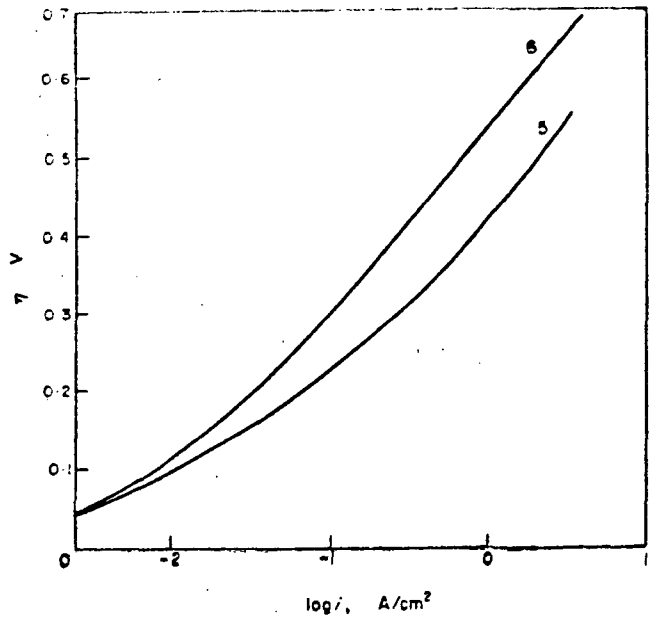

Figure 27. Current density/overpotential relationship for case where all forms of polarization are taken into account, showing effect of variation of film thickness. 5) $t = 10^{-5}$, 6) $t = 10^{-6}$ cm.

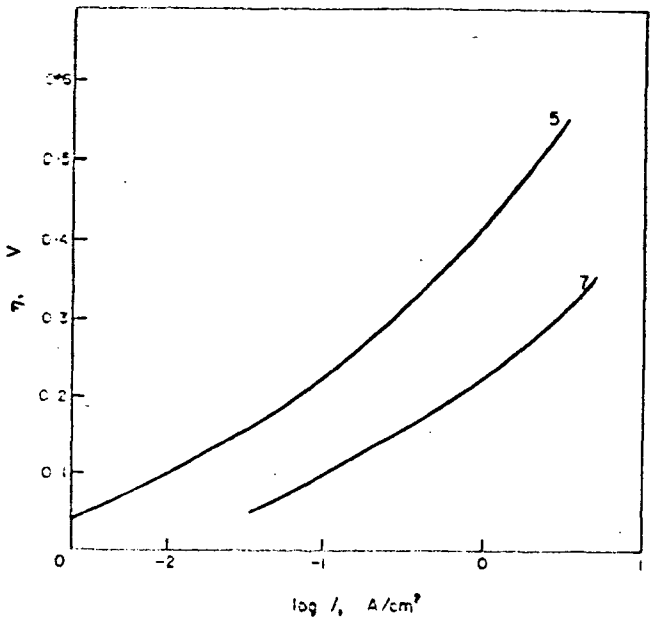

Figure 28. Current density/overpotential relationship for case where all forms of polarization are taken into account, showing effect of variation of pore radius. 5) $r = 10^{-4}$ cm, 7) $r = 10^{-3}$ cm.

The current density-overpotential relationship for the thin film model was shown to exceed those predicted by the simple pore model for the same parameter values. The performance curve exhibited a region of normal Tafel slope which passed smoothly in a double Tafel slope and finally into a region where the current density varied slowly as a function of overpotential.

The current distribution curves predicted by the thin film model were also different than predicted by the simple pore model. The simple pore model predicted a non-uniform distribution of current with overpotential; the current generation increased at either end of the pore depending on the overpotential. If the diffusivity solubility product is not high and if a limiting current is observed, the current generation predicted by the thin film model becomes non-uniform with increase in overpotential at low overpotential values, but the behavior is reversed at higher overpotentials in the regions where current is close to the limiting current. A uniform current distribution within the pore is observed at low overpotentials at the limiting current.

3. Dual Porosity Model

Many of the types of porous gas diffusion electrodes used in fuel cells have a double porosity structure: a system of gas-filled macropores superimposed on a system of liquid-filled micropores. In general, each system is composed of a distribution of pore sizes. Burshtein and co-workers (95) treated Bacon type electrodes assuming a spectrum of porosities. It was assumed that the small pores were flooded, resulting in an increase of the ionic conductivity across the electrode. This improves electrode utilization.

Grens (88) considered the macro- and micropore systems as parallel one-dimension continua joined by a series of linking pores, the length of which is short compared to the length of the micropores. This model predicted high current densities. Representative current density-overpotential curves are shown in Figure 29. The relationship between current density and overpotential predicted by the model was linear as opposed to the exponential behavior predicted by the film models. It was also shown that the extent of the gas-filled macropore system must remain large to maintain high electrode effectiveness. The electrode performance was insensitive to the linking pore length at low overpotential, but it was significantly affected by this value at high overpotentials. The effect of the linking pore length (δ) on performance is also shown in Figure 29.

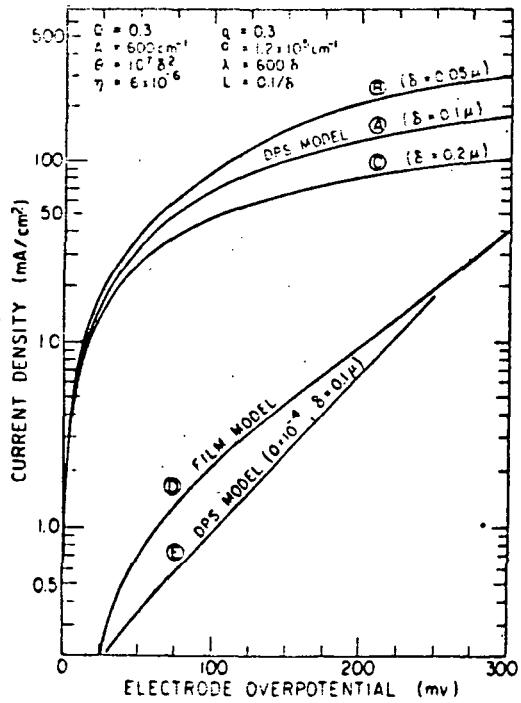

Figure 29. Calculated current density/overpotential behavior for oxygen cathode.

The reaction distribution was calculated for thin electrodes. Uniform current densities over the thickness were predicted, suggesting a very efficient use of the catalytic material.

4. Flooded Agglomerate Model

Giner and Hunter (89) pointed out some of the limitations of previously developed models of gas diffusion electrodes and presented a mathematical treatment based on substituting a column of flooded agglomerates perpendicular to the electrode surface by a porous cylinder in which catalyst particles and electrolyte were homogeneously dispersed as a continuum. During operation, it was assumed that gas diffused radially from the cylinder surface to the center with simultaneous reaction on electrocatalyst particles in the diffusion path. Ionic conduction was assumed to occur in the axial direction.

The model allowed calculation of catalyst utilization across the electrode thickness and along the radius of the flooded agglomerate. As a consequence, the importance of the agglomerate size could be evaluated in addition to porosity, bulk area, etc. It was shown that poor electrode utilization would be obtained for structures having low microporosity and large agglomerate sizes. The model further predicted regions of single and double Tafel slopes.

Electrocatalyst Utilization

It is clear from the foregoing discussion that gas diffusion electrode models are useful for examining the effect of the physical parameters of the electrode, i.e. pore size, agglomerate size, etc., on electrode performance. Guidelines for improvement of electrode structure, therefore, can be formulated based on experimental results of the electrode performance. Mass transfer of gas can be improved by changing the porosity, i.e. changing the polymer agglomerate size, and by decreasing the electrode thickness. Mass transfer of dissolved gas is improved by providing a structure where the diffusion path to the metal crystallites is short. The internal gas-electrolyte interface should also be large, suggesting high internal support area. Since chemical reaction rates generally increase proportionally with active area, the metal surface area should also be large. Increasing the active area, however, may decrease the effectiveness of the catalyst.

High surface area supported electrocatalysts are comprised of many small crystallites dispersed throughout the internal porosity of the support material. Experimental measurements of the performance of electrodes fabricated from high surface area platinum supported on carbon indicate that, for oxygen reduction in phosphoric acid, the activity of the platinum does not increase with surface area in the expected manner (96). This has been attributed to a crystallite size effect (96,97). The apparent specific platinum activity for oxygen reduction in phosphoric acid versus platinum surface area is shown in Figure 30.

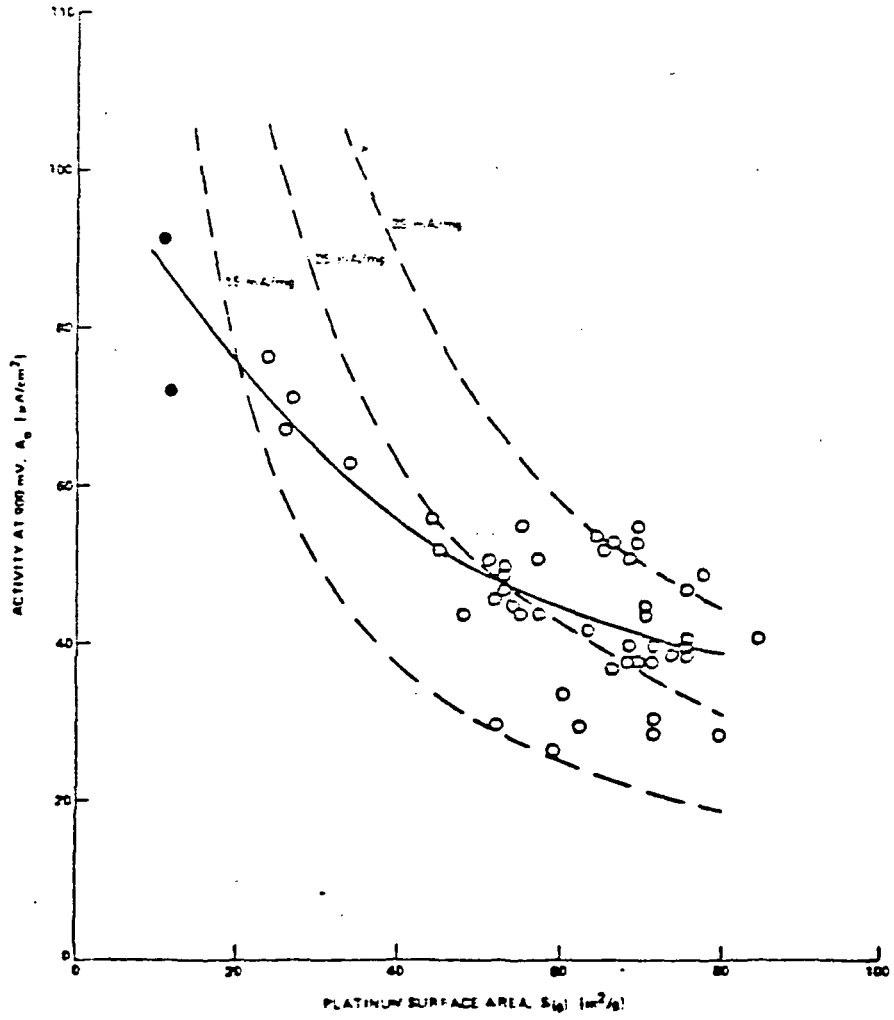

Figure 30. Specific activity as a function of surface area at 177° in 99 wt % H_3PO_4. O Platinum supported on Vulcan XC-72; ● Platinum black blended with Vulcan XC-72. The solid line is a fit of the data. The dashed lines are for constant activities per unit mass of 15, 25, and 35 mA/mg Pt.

Observed performance curves also show a decrease in measured Tafel slope (Figure 31), suggesting a change in the kinetics of the electrochemical reaction, which may also be due to a crystallite size effect. In gas phase catalysis only reactions involving the splitting of carbon-hydrogen or carbon-carbon bonds have exhibited a comparable decrease in activity with change in crystallite size (98). An alternative explanation for these observed phenomena is that the utilization of the electrocatalyst is poor.

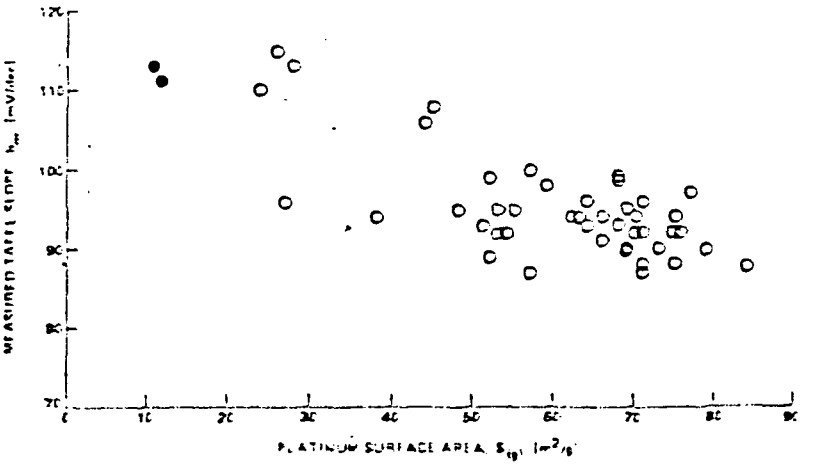

Figure 31. Variation in the measured Tafel slope as a function of platinum surface area at 177° in 99 wt % H_3PO_4. ○ Platinum supported on Vulcan XC-72. ● Platinum black blended with Vulcan XC-72.

In heterogeneous catalysis, the efficiency of a reactor or its catalyst is a common concern (99). This subject, however, has been sorely neglected by investigators in the electrocatalysis community. Since the crystallites of supported electrocatalysts are widely distributed over the surface of the substrate, it is quite likely that only part of the electrode is operating in the kinetically controlled region. Crystallites covered by hydrophobic polymer or located at unwetted pore locations will be starved for hydrogen ion and hence are controlled by the rate of ion diffusion to the active site. Other crystallites may be flooded. Here, diffusion of dissolved oxygen gas may be slow. Either situation gives rise to poor utilization of catalyst. Estimates of catalyst effectiveness have not been attempted in those studies which claim

a crystallite size effect for oxygen reduction. The only arguments posed are that linear regions in the performance curve extend over several decades of current density. If, in fact, the electrode is not operating effectively, significant performance gains can be made.

Mund and von Sturm (100) investigated the effect of electrode parameters on catalyst utilization for biporous electrodes. The degree of utilization was defined as the ratio of the transport controlled current density to the ideal current density. The effect of pore radius for overpotentials of RT/F and 4RT/F are shown in Figures 32 and 33, respectively.

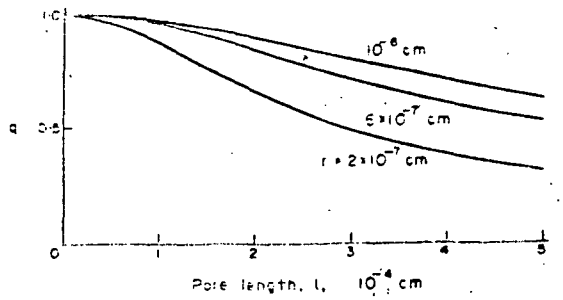

Figure 32. Degree of utilization q of the pore of a catalyst as a function of pore length l and pore radius $\eta F/RT = 1$.

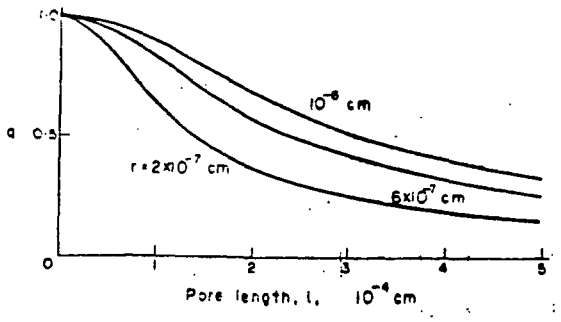

Figure 33. Degree of utilization q of the pore of a catalyst as a function of pore length l and pore radius $\eta F/RT = 4$.

In both instances, diminution of utilization with declining pore radius is perceptible. Catalyst effectiveness also decreases with increase in overpotential and increase in exchange current density. These relationships are illustrated in Figures 34 and 35.

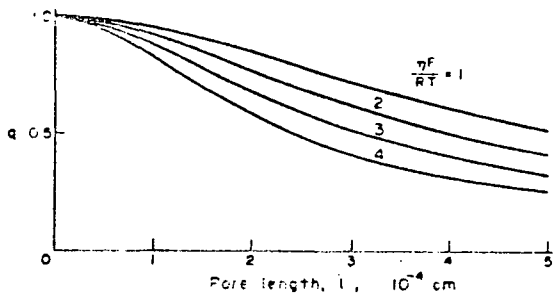

Figure 34. Degree of utilization q of the pore of a catalyst as a function of pore length l and polarization η.

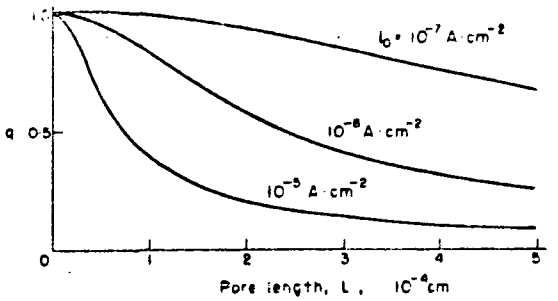

Figure 35. Degree of utilization q of the pore of a catalyst as a function of pore length l and exchange current density i_0, $\eta F/RT = 4$.

Increasing the electrode thickness was shown to decrease utilization, as expected (Figure 36).

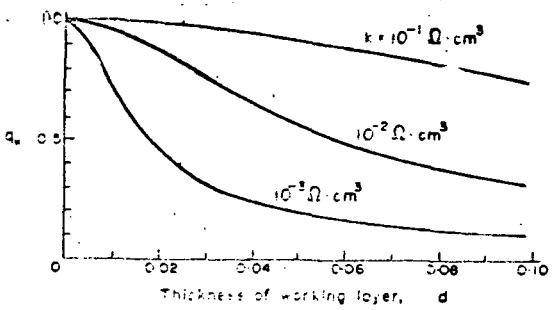

Figure 36. Degree of utilization q_w of a porous electrode as a function of thickness d of the working layer and polarization resistance k of the catalyst, the electronic resistivity has been neglected.

An approximate model for mass transfer in electrodes was derived by Cutlip (101). The model considered gaseous diffusion in the hydrophobic Teflon phase, diffusion across a thin electrolyte film at the surface of the catalyst phase, and internal diffusion with first order reaction in the electrolyte-filled catalyst phase. Analytical solutions were presented which yielded an effectiveness factor indicating the fraction of the "activation only" current obtained from the electrode. The solution allowed any combination of mass transfer processes to be important at any level of electrode operation.

In the absence of slow film diffusion, the solution was analagous to diffusion with first order reaction in a slab. The effectiveness factor relationship for this situation is illustrated in Figure 37. When film diffusion was included, catalyst effectiveness further declined. A family of curves was derived for various film moduli. The solution is presented in Figure 38. The maximum film modulus represents the case where there is no electrolyte film, i.e. a three-phase interface exists at the crystallite.

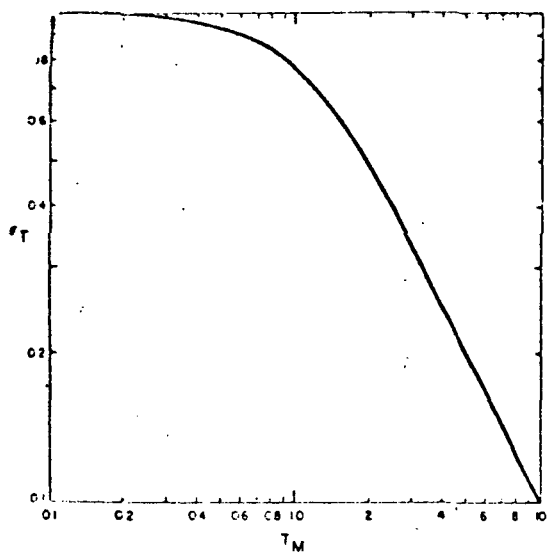

Figure 37. Effectiveness factor for reactant gas diffusion.

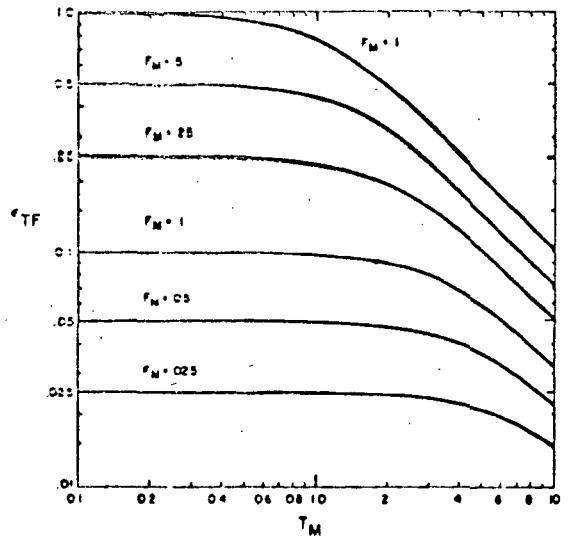

Figure 38. Effectiveness factor for gas thin film diffusion.

The model also predicted that the limiting current was related to the mass transfer processes. In the absence of gas phase diffusional losses, the limiting current was shown to be proportional to the electrode thickness. Considerable gas phase diffusional resistance yielded a limiting current which was independent of electrode thickness.

Internal diffusion with reaction in the catalyst phase was treated for slab, cylinder, and spherical geometries. The limiting current for this case was independent of the internal diffusional process in the catalyst phase.

The model was applied to a platinum black electrode for oxygen reduction in 85 w/o phosphoric acid at 120°C and 100 kPa. The oxygen partial pressure was fixed at 1%. The reduction of electrode performance due to oxygen diffusion is shown in Figure 39. Most notable is the long linear region exhibited by the curves, even though performance is far below that expected for the totally kinetic controlled situation. The importance of gaseous reactant diffusion as the limiting current is reached is illustrated in Figure 40.

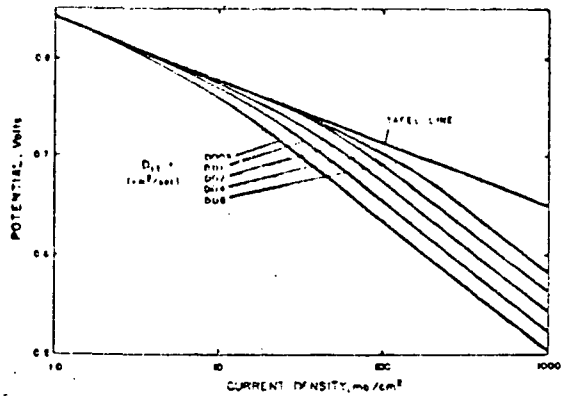

Figure 39. Gaseous diffusion losses for 1% oxygen.

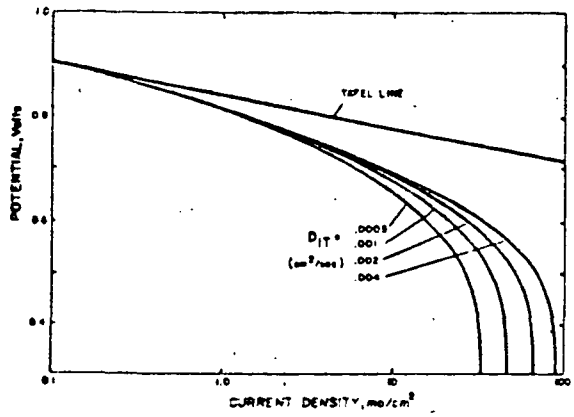

Figure 40. Effect of effective gaseous oxygen diffusion coefficient.

Performance is considerably enhanced by increase in the effective dissolved oxygen diffusion coefficient (Figure 41).

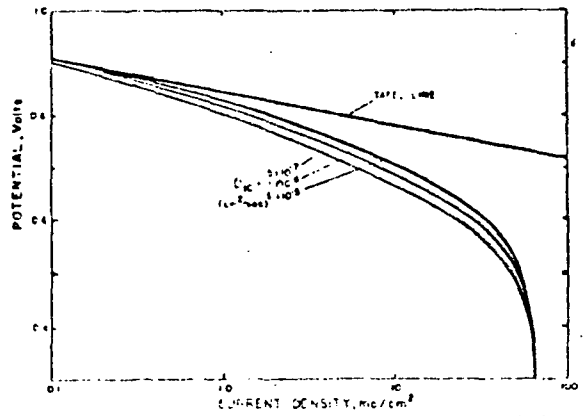

Figure 41. Effect of effective dissolved oxygen diffusion coefficient.

Performance is also improved by decreasing the agglomerate diameter as seen in Figure 42.

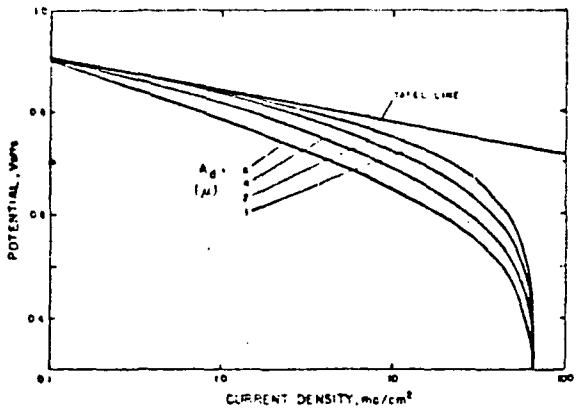

Figure 42. Effect of catalyst agglomerate diameter.

Both of these effects are due to an increase in the catalyst effectiveness factor, and neither parameter influences the limiting current of the electrode. Electrode thickness is examined in Figure 43.

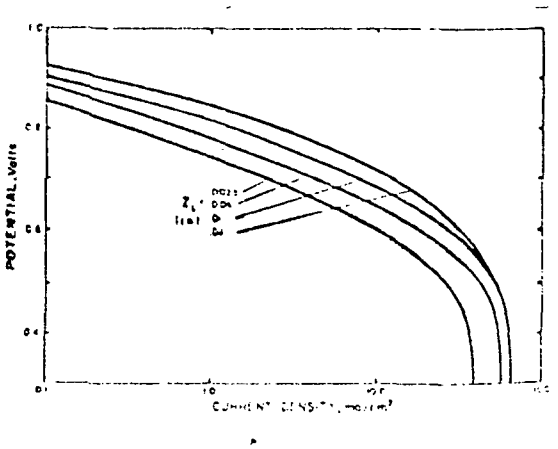

Figure 43. Effect of electrode thickness.

For this case, the catalyst loading per unit volume was held constant. It can be seen that thinner electrodes yield limiting currents which are proportional to thickness while thicker electrodes yield limiting currents independent of the thickness.

Iczkowski and Cutlip (102) later developed a multicomponent diffusion model to account for the diffusion of oxygen in the gas-filled and liquid-filled pores, electrochemical reaction, and electrical conduction in air diffusion electrodes. The model was applied to a Teflon bonded platinum on carbon electrode in acid electrolyte. Gas diffusion was shown to contribute about 38% of the voltage loss. Knudsen diffusion in the gas pores was found to be as important as molecular diffusion. Diffusion of dissolved oxygen and ohmic conduction produced only small voltage losses. It was concluded that diffusion was the major contributor to loss of catalyst effectiveness, especially at high oxygen utilization.

V. PHOSPHORIC ACID

Electrolyte management is a serious concern for long term operation of phosphoric acid fuel cells. The electrical conductivity of phosphoric acid is a strong function of concentration and, therefore, must be controlled. Since the electron transfer step in the electrochemical reaction requires that a gas-liquid-solid interface be present, dryout must be avoided. Furthermore, when acid is lost from the cell matrix, reactant gases may cross over to the opposite gas chamber. This results in a substantial drop in performance. These problems can be overcome by providing an electrolyte reservoir to replenish the acid and by treating both fuel and oxidant streams to remove acid depleting impurities, e.g. ammonia.

The electrical conductivity of phosphoric acid as a function of concentration at high temperatures is shown in Figure 44 (103) and Figure 45 (104). It is quite clear that low acid concentration is desirable to maximize electrolyte conductivity. Thermodynamic limitations, however, dictate that a high water vapor pressure exists at low acid concentration and high temperature. This means that, in the fuel cell environment, the acid concentration will tend to increase. It is not possible, therefore, to optimize performance by maximizing the electrolyte conductivity, at least with phosphoric acid. Acid concentration can be maintained by humidifying the fuel or replenishing the acid from a reservoir. Water vapor will be present in the fuel stream of reformer effluent hydrogen feeds if excess steam is used, or water vapor can be added after the fuel processing has been completed.

The matrix dryout problem can be solved by design changes. No matrix related performance declines were observed for cells operated with a matrix having high acid transport characteristics combined with regular acid addition (105).

Another method of maintaining low acid concentration (high conductivity) is to operate the cells at pressures above atmospheric. High pressure cells have been operated for extended periods with improved performance (106). High pressure cells, however, may exhibit local "hot spots" if the matrix dries out. This results in a decline of electrode performance.

The fuel cell system is likely to see a wide range of storage and operating environments, particularly for military applications. The electrolyte and other fuel cell hardware, therefore, must be capable of withstanding low temperatures.

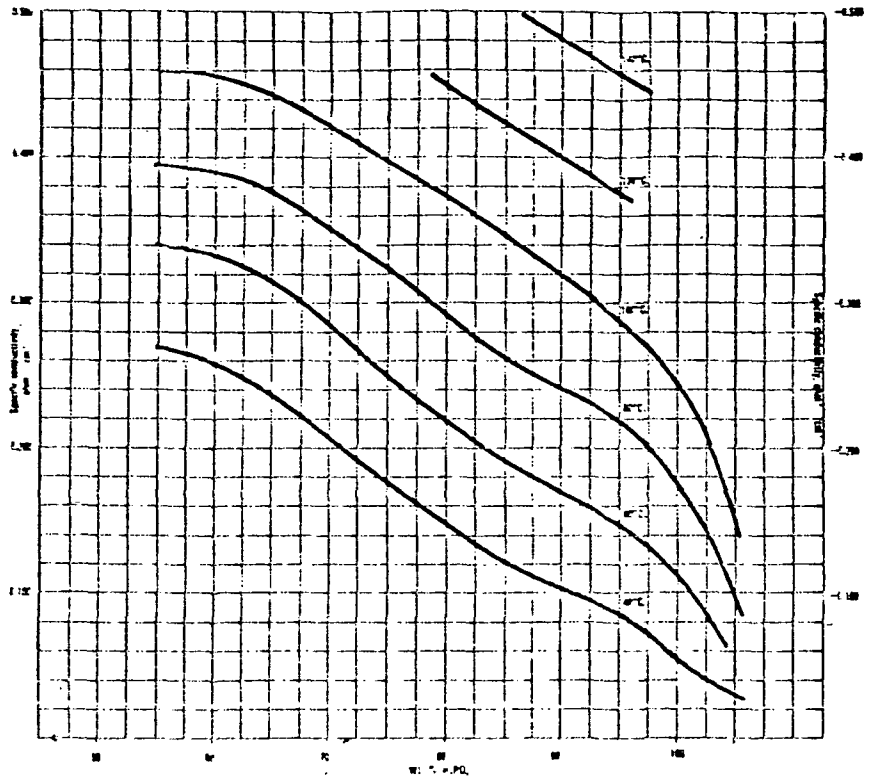

Figure 44. Electrical conductivity of phosphoric acid.

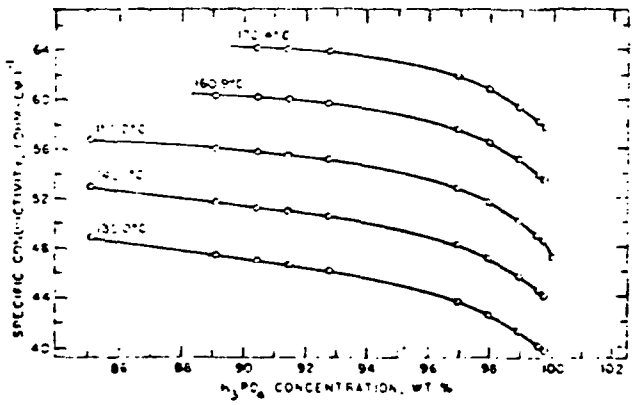

Figure 45. Electrical conductivity of phosphoric acid.

Table VI contains a list of freezing points for phosphoric acid.

TABLE VI

Freezing Points, System H_3PO_4 -H_2O

% H_3PO_4	% P_2O_5	Freezing Point °C	Freezing Point °F	Solid Phase
0	0	0	32	Ice
5	3.62	-0.8	30.6	Ice
10	7.24	-2.0	28.2	Ice
15	10.86	-3.8	25.2	Ice
20	14.48	-6.0	21.2	Ice
25	18.10	-8.6	16.5	Ice
30	21.72	-11.8	10.8	Ice
35	25.34	-15.9	3.4	Ice
40	28.96	-21.9	- 7.4	Ice
45	32.58	-30.0	-22.0	Ice
50	36.20	-41.9	-43.5	Ice
55	39.82	-58.6	-73.5	Ice
60	43.44	-76.1	-105	Ice
62.5(a)	45.25	-85.0	-121	Ice+H_3PO_4 · 1/2 H_2O
65	47.06	-70.5	- 94.9	H_3PO_4 · 1/2 H_2O
70	50.68	-43.0	- 45.5	H_3PO_4 · 1/2 H_2O
75	54.30	-17.5	0.5	H_3PO_4 · 1/2 H_2O
80	57.92	+ 4.6	40.3	H_3PO_4 · 1/2 H_2O
85	61.54	21.1	70	H_3PO_4 · 1/2 H_2O
90	65.16	28.8	83.9	H_3PO_4 · 1/2 H_2O
91.6(b)	66.32	29.3	84.7	H_3PO_4 · 1/2 H_2O
92.5	66.97	28.6	83.5	H_3PO_4 · 1/2 H_2O
94.8(c)	68.63	23.5	74.3	H_3PO_4 · 1/2 H_2O+H_3PO_4
95	68.78	24.7	76.5	H_3PO_4
97.5	70.59	34.3	93.8	H_3PO_4
100(d)	72.40	42.4	108.4	H_3PO_4
105(e)	76.02	16°C	60.8	H_3PO_4

(a) Eutectic, ice and hemihydrate.
(b) Melting point of hemihydrate, H_3PO_4 · 1/2 H_2O.
(c) Eutectic, H_3PO_4 · 1/2 H_2O and H_3PO_4.
(d) Melting point of anhydrous acid, H_3PO_4.
(e) Pure H_3PO_4 crystallizes rather slowly. It is very easy to supercool a concentrated acid such as 105% H_3PO_4 to obtain a glassy substance.

Examination of the table indicates that for acid concentrations of interest for fuel cell application, temperatures greater than 25°C are required for phosphoric acid to remain liquid. The acid, however, does not solidify rapidly and can remain liquid at temperatures as low at -17°C. If the electrolyte does, in fact, freeze, damage to the electrodes may occur resulting in unacceptable performance declines during operation following the thaw cycle.

The freeze damage is due largely to flooding of the electrodes. Electrodes which are not completely filled with electrolyte will tolerate 2-3 freeze cycles without serious performance loss (106). The procedure for testing freeze tolerance is to seal fuel and oxidant lines at open circuit while lowering the temperature to the desired level. The cell system is held at freeze temperature (about -32°C) for three days. Following the three-day freeze, the stack is thawed to about 25°C and then raised to operating temperature. Performance loss can generally be attributed to flooding of the electrodes during the freeze.

Three solutions have been proposed to reduce freeze damage to the electrodes (106). The electrolyte can be wetted to a concentration that does not freeze at the storage temperature. Once the cell is restarted, equilibrium factors will cause the acid concentration to return to normal operating levels. The electrolyte can also be dried out. This results in a reduction of volume and an increase in the viscosity of the phosphoric acid -- conditions which would tend to reduce the probability of electrolyte penetration into the pores of the electrocatalyst. A final method is to increase the hydrophobicity of the electrodes, thereby decreasing the wetting characteristics. When the latter method is employed, care must be taken so that the electrocatalytic behavior is not changed by addition of the hydrophobic material. Both the wetting and hydrophobicity methods have resulted in diminished performance loss.

It is well known that electricity demand during the course of a 24 hour period is cyclic. The response of the fuel cell to load cycling, therefore, is also of interest. Long-term performance declines have been observed for start-up/shutdown cycling (105). The decline was attributable to breaching of the electrolyte matrix. It was believed that this was caused by transient operation of the stack. Load cycling to follow electrical demand would result in breaching problems, hence performance decline.

Only modeling of acid evaporation and acid loss due to reaction with impurities has been undertaken. Both models perform well in predicting the long-term effects on performance. The freeze/thaw and load cycling phenomena appear to be correctable by materials and/or operational modifications, so mathematical models are unnecessary.

VI. IMPURITY EFFECTS

Recent advances in hydrocarbon fuel processing have widened the range of fuels from which hydrogen can be obtained (107,108). The variety of impurities, therefore, has also expanded. How the fuel cell responds to impurities determines the level of sophistication required for fuel clean-up and construction of cell components. The literature on long-term impurity effects is sparse with the exception of the effects of those contained in the fuel or produced during fuel processing. Based on the work conducted to date, Table VII shows the impurity levels that can be tolerated in phosphoric acid fuel cells without suffering significant performance decline (109,110).

Hydrocarbon impurities are produced in the steam reforming process and are of importance at the anode. Naphtha, No. 2 fuel oil, and now possibly heavy liquid fuels derived from coal and shale oil are used for the manufacture of hydrogen fuel. Concurrent with the steam reforming reactions are the water-gas shift and methanation reactions. Also, natural gas feedstocks will contain small amounts of unreacted methane, or methane formed from the higher hydrocarbons which make up natural gas. Traces of C_2 and higher hydrocarbons may also be present for the liquid fuels, since both steam cracking and catalytic cracking may occur (111). Long term testing of these impurities has been reported for methane only (112). Fuel cells were subjected to feed streams containing up to 15% methane for periods of up to 5,000 hours duration. The only effect was apparently a diluent effect, the drop in performance attributed to lower hydrogen composition. The anode electrocatalysts were analyzed by electron microscopy and cyclic voltammetry, and the electrolyte was chemically analyzed at the conclusion of the test. These analyses confirmed that methane was both chemically and electrochemically inert. The longer-chain hydrocarbons exhibit poisoning effects at the anode (110). This is probably due to chemisorption by C-C bonds on multiple platinum sites. Any reactions of these adsorbed entities will be slow, hence the catalyst will show an apparent decrease in activity. There have been no reported in-depth studies concerning the long term effects of C_2 and higher hydrocarbon compounds on fuel cell performance. Up to now, steam reforming technology for naphthas and other light and middle distillate fuels is available to produce fuel cell feeds containing only trace quantities of these species. Nevertheless, future use of liquids derived from shale or residuum oils could increase the impact of these hydrocarbons on long term fuel cell performance. Advances in steam reforming may be required to keep the hydrocarbon level below 100 ppm.

TABLE VII

Maximum Allowable Impurity Levels for Phosphoric Acid Fuel Cells

Impurity	Limit
Hydrocarbons	
CH_4	dil.
C_2 and higher	100 ppm
Carbon	
CO	4%[1]
CO_2	dil.
Nitrogen	
N_2	dil.
NH_3	.1-1 ppm
Sulphur	
COS	100 ppm
H_2S	100-200 ppm
Metals	
Fe	trace
V	trace
Cu	trace
Others	
Cl^-	1 ppm
H_2O	dil.

[1] CO tolerance is a function of temperature so operating conditions will determine maximum allowable concentration.

Other carbon based impurities will be present in anode feeds, namely CO and CO_2. Like the hydrocarbon impurities, these gases are also produced during reforming. Shift converters remove carbon monoxide which seriously diminishes the performances of anode electrocatalysts. Carbon dioxide, on the other hand, acts only as a diluent. Anode poisoning by carbon monoxide occurs by site elimination (113). The apparent Pt activity is decreased and anode polarization is increased substantially. Recent developments in fuel cell materials have resulted in an increase of operating temperature to the 180-200°C range. The threshold limit reported in Table VII is for 160°C. Since CO poisoning is dependent on temperature (see Figure 46), this change of operating conditions to higher temperatures will allow tolerance of higher CO feed concentrations. Novel alloy electrocatalysts have been shown to be superior to platinum for up to 30% CO anode feeds at 180°C (114), and further increases in temperature may eliminate CO from consideration as an impurity problem. The long term effects of CO poisoning are reversible when the carbon monoxide is removed from the feed (115). Synergistic effects of carbon monoxide and other impurities are discussed later.

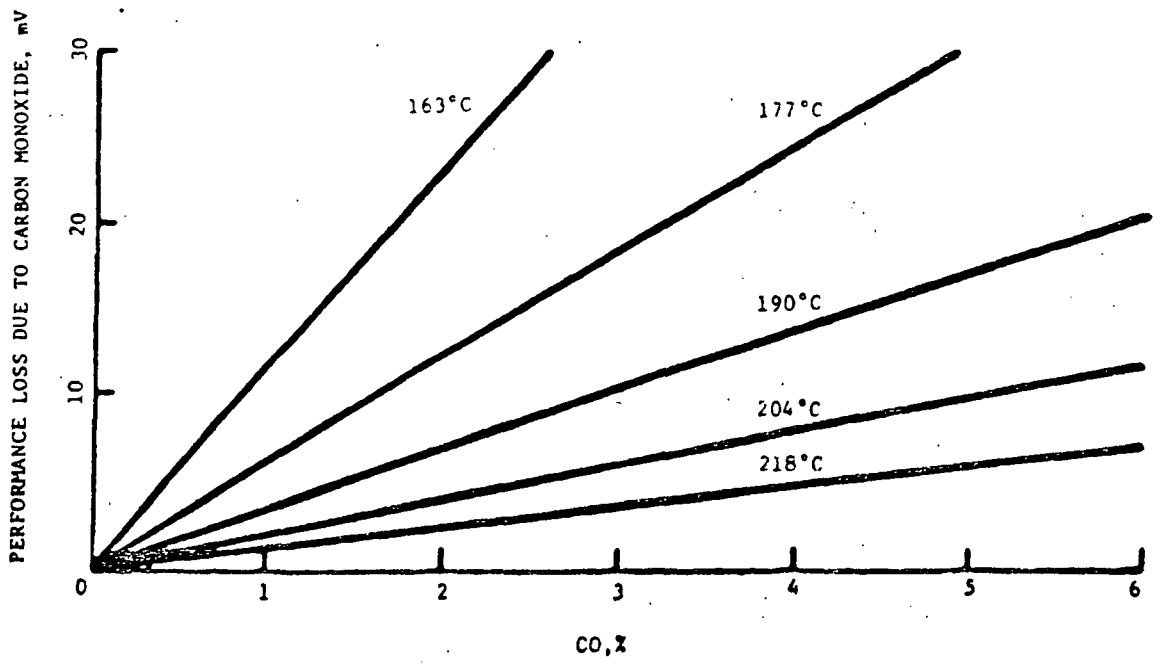

Figure 46. Effect of CO content and temperature on anode performance. 0.35 mg Pt/cm^2, 269 mA/cm^2.

Nitrogen compounds enter the fuel cell with both fuel and oxidant streams. Air is used as the oxidant so nitrogen gas is present in large quantities at the cathode. The nitrogen acts only as a diluent; no long term deleterious effects have been observed. The diluent effect of nitrogen gas is also observed at the anode. Here, nitrogen is generally introduced by nitrogen containing hydrocarbons. Compounds such as NH_3, HCN, and NO_x, however, may also be formed. These nitrogen containing compounds may still be produced even if nitrogen-free feedstocks are used if the fuel processing scheme includes autothermal reforming or coal gasification (107). All of these nitrogen compounds result in decreased fuel cell performance. The available literature deals largely with the problems associated with the introduction of ammonia.

Ammonia reacts with phosphoric acid to form ammonium dihydrogen phosphate. Very low levels of ammonia can be tolerated in the fuel cell without noticeable performance loss (112). If the phosphoric acid is ammoniated to greater than 0.2 mole %, significant performance loss is observed (116). Various theories have been advanced to explain the performance decrease (110). Among them are poisoning of the platinum at the cathode and decrease of the conductivity of the acid. In the work of Szymanski, et al (116), an 84% loss of "cathode activity" was reported for 1% conversion of acid to ADHP. This was believed to occur because of oxidation of ammonium ion at the cathode. A conductivity decrease theory, however, would also account for this performance decrease. For oxygen reduction to occur, hydrogen ion must migrate from the anode to the cathode. Regardless of the mode of transfer (diffusion of H^+ or proton chain conduction, for example), a decrease in solution conductivity lowers the H^+ concentration at the cathode resulting in a concomitant decrease in performance. Long term performance testing has been conducted to determine the effects of sustained introduction of ammonia. Constant levels of ADHP were reached, but these concentrations were much lower than would be predicted on the basis of complete conversion of inlet ammonia concentrations. This result, coupled with the fact that performance can be restored on removal of ammonia from the feed (see Figure 47) leads to the conclusion that the ammonium ion can be oxidized at the cell operating conditions.

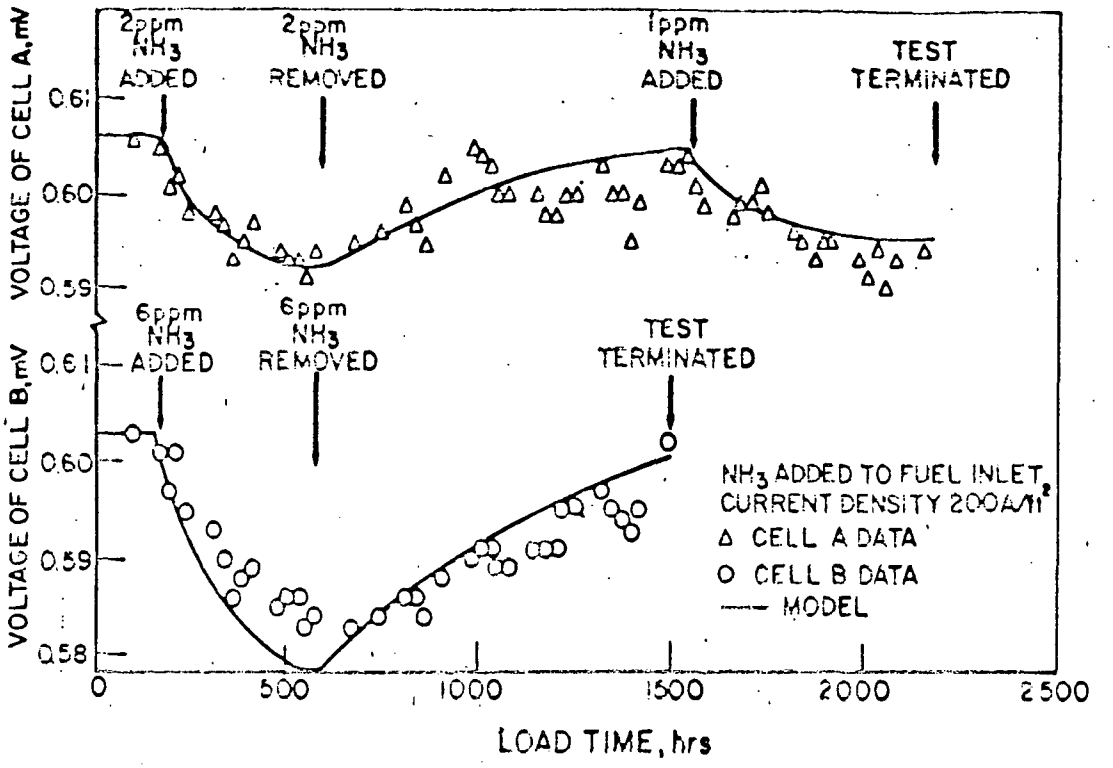

Figure 47. Cell endurance in the presence of ammonia.

Advanced fuel processors operating on petroleum or coal derived liquid fuels produce H_2S. An adiabatic reformer using No. 2 fuel oil, for example, is expected to produce an anode fuel containing about 320 ppm H_2S (117). This gaseous sulphur compound must be removed before the fuel reaches the cell stack. Sulphur compounds severely poison platinum based electrocatalysts. The introduction of 130 ppm H_2S to cells operating at 205°C caused rapid performance decay (115) after a short period of stable operation. Similar behavior was observed for 180 ppm H_2S at 190°C (118). Stable operation was observed for about 400 hr in this test before performance decayed rapidly. In general, operation of fuel cells on fuels containing ppm quantities of H_2S are characterized by periods of stable operation followed by rapid performance decreases (110). Original performance can be restored by removing H_2S from the feed as shown in Figure 48. As with carbon monoxide, the poisoning apparently occurs by site elimination. Improved tolerance to sulphur compounds has been reported for temperatures in excess of 200°C (118).

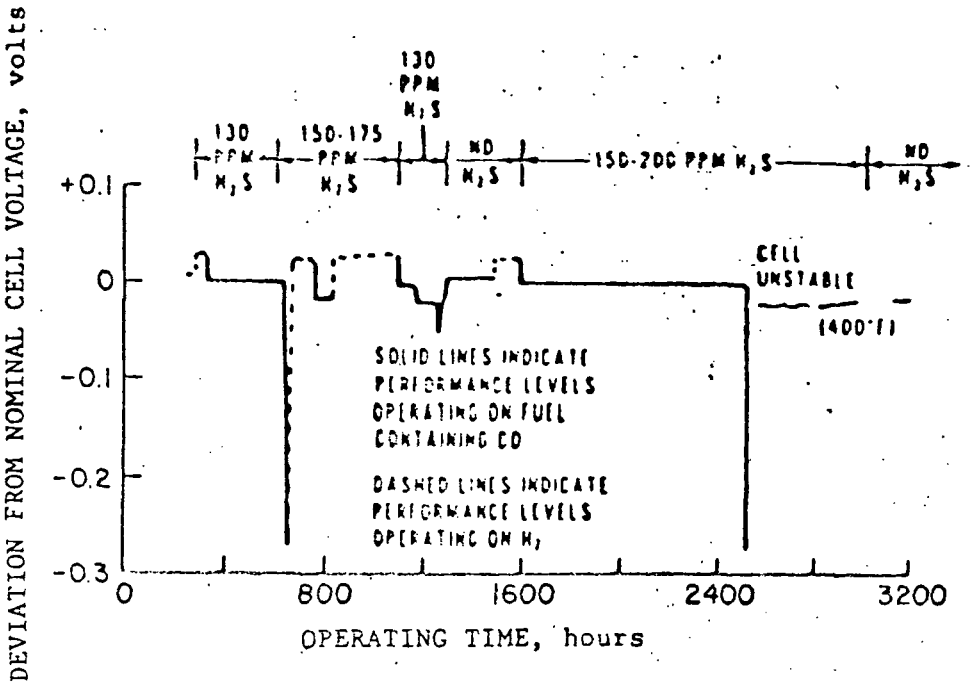

Figure 48. Effect of H_2S on phosphoric acid fuel cell performance.

Operation of cell stacks on fuels containing both CO and H_2S has also been examined (115). Rapid decay is observed following introduction of these poisons to the cell stack. Original performance can be approached or restored completely by removing either CO or H_2S or both. This provides strong evidence for a synergistic effect between these poisons. Thermodynamic calculations indicate that about 0.5 ppm carbonyl sulphide would be in equilibrium with a simulated reformer effluent containing 200 ppm H_2S. It is conceivable, therefore, that COS is formed on the anode by reaction between CO and H_2S. Several tests have been run with 1 ppm COS added to the fuel, but no observable performance loss attributable to COS was observed in the temperature range 175-200°C (118). It is clear from this observation that H_2S-CO interaction with the electrocatalyst is complex and, at this time, far from being understood.

Electrodes exposed to sulphur concentrations for long time periods have been examined to identify any structural changes which could be attributed to the sulphur alone. No observable changes in the electrodes could be detected and no changes in catalyst properties were found (115).

Poisoning of electrocatalysts by metals may also occur. The steam reforming and shift conversion catalysts are subject to physical degradation. It would be expected, therefore, that trace quantities of metals such as nickel, copper,

and zinc might be introduced in the fuel stream. Vanadium is known to be present in middle and heavy distillate fuel and may cause serious problems if residuum fuels are used (119). Iron and copper metals can be leached from hardware if protective coatings are etched. Large polarization (above 50 mV) has been attributed to copper poisoning (107). Finally, iron is also present in carbon and can be leached, for example, from the graphite end plates.

VII. CONCLUSIONS AND RECOMMENDATIONS

This review has focused on the identification of processes that effect the long term stability of electrodes in phosphoric acid fuel cells. Loss of active catalytic surface area, corrosion of the carbon electrocatalyst support, electrocatalyst utilization, electrode structure degradation, degradation of electrolyte, and impurity effects have been discussed in this regard. No study has been conducted with the purpose of developing a model capable of predicting the long term effects of any of these processes on the basis of short term tests. Farooque and co-workers (120) attempted to model long term cell stack performance using empirical decay parameters. The decay parameters were determined by regression analysis of the results of perturbation experiments. Since the model was entirely empirical, no knowledge as to the underlying processes which contribute to performance declines was obtained. It is not likely, therefore, that models of this type will be universally reliable tools for prediction of long term performance.

The results of the survey on electrolyte degradation indicate that, with appropriate electrolyte management schemes, no loss in electrode performance will occur. The mechanism by which ammonia contributes to the degradation of phosphoric acid fuel cell performance is still open for debate. Elucidation of this mechanism may be required in view of the success of autothermal reforming and the likelihood that heavy hydrocarbon fuels may be the source of hydrogen.

In addition to ammonia as an impurity, carbon monoxide and hydrogen sulphide are particularly deleterious to electrode performance. Tolerance to carbon monoxide has been increased by raising the fuel cell operating temperature, and new catalysts have been developed that perform better than platinum at relatively high CO levels (114). Furthermore, a recent study of the economics of phosphoric acid fuel cell power plants suggests that elimination of the shift converters currently employed for reduction of carbon monoxide feed compositions would not result in significant capital cost savings (121). The development of sulphur tolerant electrocatalysts is not likely to have a large impact on the technology of fuel cells. Sulphur emissions standards are quite strict; therefore the sulphur will have to be removed somewhere in the system. It would appear more prudent to use the desulphurization technology available from the petroleum industry to remove sulphur from the hydrocarbon feedstock, particularly since the steam reforming catalysts are also susceptible to sulphur poisoning.

Review of the extant literature on carbon corrosion suggests that the mechanism of this decay process is understood, and techniques have been developed for accelerated testing of new support materials (58). Stable supports require at least some ordering of the surface structure to be useful over the expected lifetime of the fuel cell system. The interaction of the support with platinum crystallites is not understood. The concept of trap sites was suggested by Bett, et al (56) as a mode of sintering retardation. The possibility of purposely introducing "trap sites" into the carbon surface through controlled modification of the support is intriguing. Indeed, work on this concept is ongoing, e.g. the work of Remick (64), and should continue.

Although much time and effort has been expended toward elucidation of the processes which contribute to surface area loss of platinum electrocatalysts, no clear identification of the sintering mechanism in phosphoric acid has been identified. The lack of success in the development of stable electrocatalysts points out the need for clearly understanding the physical processes which cause long term performance decay. Perhaps the most definitive study on the subject of surface area loss was conducted by Gruver, et al (59). Electron microscopy was used extensively in this investigation. Recently, Baker has suggested the use of electron microscopy for in situ studies of catalyst sintering in gas phase environments (122). Similar experiments can be conceived for the phosphoric acid environment. It remains to be seen whether a suitable "electrochemical reactor" can be designed for this purpose, however.

Since the capital investment for the cell stack in phosphoric acid fuel cell power plants is about 40% of the total plant investment, the greatest impact on fuel cell feasibility arises from dramatic improvement in power density. Such an improvement would lead to a proportional decrease in stack size, and, therefore, stack cost. It is not clear that the platinum electrocatalyst is being utilized effectively. How long term structure degradation affects utilization is also not known. Recent evidence suggests that the cathode operates at only about 65% effectiveness (81), even though it is usually argued that this electrode operates in the kinetic controlled regime. The importance of the work of Cutlip (101) has not been realized, and definitive studies in this area are still required. The use of transient techniques should contribute to a clearer understanding of the operation of porous gas diffusion electrodes. The value of these methods in elucidating transport and reaction mechanisms is well known (123).

As a further aid to understanding platinum utilization, it is necessary to develop in situ surface area measurement methods so that the platinum available for reaction under actual operating conditions can be estimated. The standard electrochemical hydrogen adsorption method is not applicable at these conditions since hydrogen evolution interferes with the adsorption peak (124). Comparison of platinum surface as measured under reaction conditions with that measured by room temperature electrochemical adsorption will provide valuable information concerning the location of platinum crystallites in the electrode structure. Appropriate modifications in both catalyzation procedures and electrode fabrications can then be devised.

BIBLIOGRAPHY

1. J. H. Sinfelt, Annu. Rev. Mat. Sci. 2, 641 (1972).
2. J. E. Benson and M. Boudart, J. Cat. 4, 704 (1965).
3. M. A. Vannice, J. E. Benson, and M. Boudart, J. Cat. 16, 348 (1970).
4. K. Kinoshita, K. Routsis, J. A. S. Bett, and C. S. Brooks, Electrochim. Acta 18, 953 (1973).
5. P. A. Sermon, J. Cat. 24, 460 (1972).
6. J. C. Schlatter in Sintering and Catalysis, G. C. Kuczynski, ed., Plenum Press, N.Y., 141 (1975).
7. A. P. Fickett in Electrode Materials and Processes for Energy Conversion and Storage, J. D. E. McIntyre, S. Srinivasan, and F. G. Will, The Electrochemical Society, Inc., Princeton, N.J., 546 (1977).
8. J. A. S. Bett, K. Kinoshita, and P. Stonehart, J. Cat. 41, 124 (1976).
9. K. Kinoshita, J. A. S. Bett, and P. Stonehart in Sintering and Catalysis, G. C. Kuczynski, ed., 117 (1975).
10. K. Kinoshita, in The Electrocatalysis of Fuel Cell Reactions, W. E. O'Grady, S. Srinivasan, and R. F. Dudley, The Electrochemical Society, Inc., Princeton, N. J., 144 (1978).
11. S. E. Wanke and P. C. Flynn, Cat. Rev.-Sci. Eng. 12, 93 (1975).
12. E. Ruckenstein and B. Pulvermacher, AIChE J. 19, 356 (1973).
13. E. Ruckenstein and B. Pulvermacher, J. Cat. 29, 224 (1973).
14. P. Wynblatt and N. A. Gjostein, Scr. Met. 7, 969 (1973).
15. P. Wynblatt and N. A. Gjostein, Prog. Solid State Chem. 9 (1974).
16. P. C. Flynn and S. E. Wanke, J. Cat. 34, 390 (1974).
17. P. C. Flynn and S. E. Wanke, J. Cat. 34, 400 (1974).
18. M. von Smoluchowski, Z. Phys. Chem. 92, 129 (1918).
19. W. Ostwald, Z. Phys. Chem. 34, 495 (1900).
20. A. B. Shekhter, A. I. Echeistova, and I. I. Tret'yakov, Izv. Akad. Nauk SSSR Otd. Khim. Nauk., 465 (1950).
21. T. P. Kobylinski, B. W. Taylor, and J. A. Young, SAE Meeting Det. (1974).
22. W. P. Pierson, R. H. Hammerle, and J. T. Kummer, SAE Meeting Det. (1974).
23. J. C. Chaston, Plat. Met. Rev. 8, 50 (1964).
24. E. R. Plante, A. B. Sessoms, and K. R. Fitch, J. Res. Nat. Bur. Stand., A 74, 647 (1970).
25. J. A. Pask and R. M. Fulrath, J. Amer. Chem. Soc. 45, 592 (1962).

26. M. Humenik and W. D. Kingery, J. Amer. Chem. Soc. 37, 18 (1954).

27. G. A. Bassett in Condensation and Evaporation of Solids, E. Ruther, P. Goldfinger, and J. P. Hirth, eds., Gordon and Breach, N.Y. (1964).

28. W. B. Phillips, E. A. Desloge, and J. G. Skofronick, J. Appl. Phys. 39, 3210 (1968).

29. A. Masson, J. J. Metois, and R. Kern, Surf. Sci. 27, 463 (1971).

30. R. Kern, A. Masson, and J. J. Metois, Surf. Sci. 27, 483 (1971).

31. J. M. Thomas and P. L. Walker, J. Chem. Phys. 41, 587 (1964).

32. P. C. Flynn and S. E. Wanke, J. Cat. 37, 432 (1975).

33. J. W. Geus in Chemisorption and Reactions on Metallic Films, J. R. Anderson, ed., Academic Press, N.Y. (1971).

34. B. Pulvermacher and E. Ruckenstein, J. Cat. 35, 115 (1974).

35. D. L. Swift and J. Friedlander, Colloid. Sci. 19, 621 (1964).

36. H. J. Maat and L. Moscou, Proc. 3rd Int. Cong. Cat., North Holland, Amsterdam (1965).

37. R. A. Herrmann, S. F. Adler, M. S. Goldstein, and R. M. DaBaun, J. Phys. Chem. 65, 2189 (1961).

38. J. A. S. Bett, K. Kinoshita, and P. Stonehart, J. Cat. 35, 307 (1974).

39. F. S. Stone, Adv. Cat. 13, 1 (1962).

40. F. Solymosi, Cat. Rev.-Sci. Eng. 1, 233 (1967).

41. J. Escard, B. Pontvianne, and J. P. Contour, J. Electron Spec. 6, 17 (1975).

42. J. Escard, C. Leclere, and J. P. Contour, J. Cat. 29, 31 (1973).

43. C. S. Nicolau, H. G. Thom, and E. Pobitschka, Trans. Far. Soc. 55, 1430 (1959).

44. L. J. Hillenbrand and J. W. Lacksonen, J. Electrochem. Soc. 112, 249 (1965).

45. N. M. Sagert and R. M. L. Ponteau, Can. J. Chem. 50, 3686 (1972).

46. G. Bohme, P. Hohn, H. Krupp, H. Rabenhorst, and G. Walter, J. Appl. Phys. 44, 3914 (1973).

47. A. D. Zimon, Adhesion of Dust and Powder, Plenum Press, N.Y. (1969).

48. D. G. Tabatadze, I. A. Myansikov, and L. A. Evstigneeva, Russ. J. Phys. Chem. 46, 1488 (1972).

49. J. C. Anderson, ed., Electron Transport in Thin Metal Films, Academic Press, N.Y. (1966).

50. D. McKee, J. Phys. Chem. 67, 841 (1963).

51. S. Khassan, S. Fedorkina, G. Emel'ynova, and V. Lebedev, Zh. Fiz. Khim. SSSR, 42, 2507 (1968).

52. P. Stonehart and P. Zucks, Electrochim. Acta 17, 2333 (1972).

53. J. F. Connolly, R. J. Flannery, and B. L. Meyers, J. Electrochem. Soc. 114, 241 (1967).

54. A. C. C. Tseung and S. C. Dhara, Electrochim. Acta 20, 681 (1975).

55. K. F. Blurton, Carbon 10, 305 (1972).

56. J. A. S. Bett, K. Kinoshita, K. Routsis, and P. Stonehart, J. Cat. 29, 160 (1973).

57. A. C. C. Tseung, Proc. Fuel Cell Catalysis Workshop, Palo Alto (1975).

58. P. Stonehart and J. P. MacDonald, EPRI EM-1664 (1979).

59. G. A. Gruver, R. F. Pascoe, and H. R. Kunz, J. Electrochem. Soc. 127, 1219 (1980).

60. K. F. Blurton, H. R. Kunz, and D. R. Rutt, Electrochim. Acta 23, 183 (1978).

61. J. M. Thomas in Chemistry and Physics of Carbon, P. L. Walker, ed., 1, 121 (1965).

62. D. W. McKee, Carbon 8, 623 (1970).

63. D. W. McKee, Carbon 8, 131 (1970).

64. R. J. Remick, DOE Contract DEN-3-208 2nd Quarterly (1981).

65. Y. C. Pan and G. Ciprios, EPRI EM-661 (1978).

66. Y. C. Pan and G. Ciprios, EPRI EM-833 (1978).

67. L. B. Welsh, R. W. Leyerle, D. S. Scarlata, and M. A. Vanek, EPRI EM-1711 (1981).

68. W. R. Smith in Encyclopedia of Chemical Technology, Interscience, N.Y. (1964).

69. A. S. Behrmann and H. Gustafson, Ind. Eng. Chem. 27, 426 (1935).

70. N. M. Winslow, Trans. Electrochem. Soc. 92, 411 (1947).

71. J. B. Donnet, F. Hueber, C. Reitzer, J. Oddoux, and G. Reiss, Bull Soc. Chim. France 1727 (1962).

72. W. Stegemann and R. Meyer, Ger. Pat. 892,493 (1953).

73. B. R. Puri, O. P. Mahajan, and D. D. Singh, J. Indian Chem. Soc. 38, 135 (1961).

74. J. B. Donnet and G. Henrich, Bull. Soc. Chim. France 1609 (1960).

75. U. Hoffmann and G. Ohlerich, Angew. Chem. 62, 16 (1950).

76. H. Binder, A. Kohling, K. Richter, and G. Sandstede, Electrochim. Acta 9, 255 (1964).

77. L. J. J. Janssen and J. G. Hoogland, Electrochim. Acta 15, 339 (1970).

78. J. B. Donnett and P. Ehrburger, Carbon 8, 697 (1970).

79. R. E. Panzer and P. J. Elving, Electrochim. Acta 20, 635 (1975).

80. K. Kinoshita and J. A. S. Bett, Carbon 11, 237 (1973).

81. L. Christner and M. George, DOE Contract DE-AC-03-78ET13114 (1981).

82. K. E. Gubbins and R. D. Walker, Jr., J. Electrochem. Soc. 112, 469 (1965).

83. K. Klinedinst, J. A. S. Bett, J. MacDonald, and P. Stonehart, Electroanal. Chem. and Inter. Electrochem. 57, 281 (1974).

84. E. W. Justi and A. W. Winsel, Kalte Verbrennung Franz Steiner Verlag, GmbH, Wiesbaden (1962).

85. F. G. Will, J. Electrochem. Soc. 110, 145 (1963).

86. R. Buvet and S. Palous, Bull. de la Soc. Chimique de France, 1602 (1962).

87. L. G. Austin, M. Mariet, R. D. Walker, Jr., G. B. Ward, and R. H. Comyn, I & EC Fund. 4, 321 (1965).

88. E. A. Grens II, I & EC Fund. 5, 542 (1966).

89. J. Giner and C. Hunter, J. Electrochem. Soc. 116, 1124 (1969).

90. H. H. Horowitz, J. Electrochem. Soc. 114, 650 (1967).

91. S. Srinivasan, H. D. Hurwitz, and J. O'M. Bockris, J. Chem. Phys. 46, 3108 (1967).

92. D. A. J. Swinkels, J. Electrochem. Soc. 113, 6 (1966).

93. L. G. Austin, Report No. 3, Contract DA-49-186-502-ORD-917 (1962).

94. S. Srinivasan and H. D. Hurwitz, Electrochimica Acta 12, 495 (1967).

95. R. C. Burshtein, V. X. Markin, A. G. Psenichnikov, V. A. Chismadgev, and Y. G. Chirkov, Electrochim. Acta 9, 773 (1964).

96. L. J. Bregoli, Electrochim. Acta 23, 489 (1978).

97. H. R. Kunz in The Electrocatalysis of Fuel Cell Reactions, W. E. O'Grady, S. Srinivasan, and R. F. Dudley, eds., The Electrochemical Society, Inc., Princeton, N.J. (1978).

98. M. Boudart, A. Aldag, J. E. Benson, N. A. Dougherty, and C. G. Harkins, J. Cat. 6, 92 (1966).

99. C. W. Satterfield, Mass Transfer in Heterogeneous Catalysis, MIT Press, Cambridge (1970).

100. K. Mund and F. von Strum, Electrochimica Acta 20, 463 (1974).

101. M. B. Cutlip, Electrochimica Acta 20, 767 (1975).

102. R. P. Iczkowski and M. B. Cutlip, J. Electrochem. Soc. 127, 1433 (1980).

103. Monsanto Technical Bulletin IC/DP 239.

104. D. I. MacDonald and J. R. Boyack, J. Chem. Eng. Data 14, 380 (1969).

105. A. Kaufman and P. Terry, U.S. MERADCOM, DAAK 70-77-C-0206 (1980).

106. R. D. Breault, J. V. Congdon, R. D. Coykendall, W. L. Luoma, D. L. Maricle, A. P. Mientek, J. O'Brien, and R. D. Sawyer, DOE DE-AC-03-76-ET-11301 (1979).

107. ———————— Catalytica Associates EPRI EM 570 (1977).

108. ———————— Arthur D. Little, Inc. EPRI EM 695 (1978).

109. R. G. Minet and D. Warren, KTI Corp. EPRI EM 1487 (1980).

110. T. G. Benjamin, E. H. Camara, and L. G. Marianowski, DOE EC-77-C-03-1545 (1980).

111. C. R. Schnell, J. Chem. Soc. (B) 158 (1970).

112. J. M. King, EPRI EM 335 (1976).

113. G. Kohlmayer and P. Stonehart, Electrochimica Acta 18, 211 (1973).

114. P. Stonehart, J. Baris, J. K. Hochmuth, and P. Pagliaro, DOE-0176 (1981).

115. J. M. King, EPRI EM 576 (1977).

116. S. T. Szymanski, G. A. Gruver, M. Katz, and H. R. Kunz, J. Electrochem. Soc. 127, 1440 (1980).

117. J. A. S. Bett, C. L. Bushnell, R. F. Buswell, G. A. Gruver, J. M. King, and H. R. Kunz, EPRI EM 1328 (1980).

118. W. E. Houghtby, J. M. King, and R. A. Thompson, EPRI EM 956 (1978).

119. B. C. Gates, J. R. Katzer, and G. C. A. Schuit, Chemistry of Catalytic Processes, McGraw Hill, N.Y. (1979).

120. M. Farooque, H. Maru, and D. Patel, DOE DE-AC05-79ET15381 (1980).

121. A. Levy and L. VanDine, FCR 1737 (1980).

122. R. T. K. Baker, Cat. Rev.-Sci. Eng. 19, 161 (1979).

123. J. K. Hochmuth, Ph.D. Thesis University of Connecticut (1981).

124. W. E. O'Grady, H. Olender, H. S. Isaacs, and S. Srinivasan, Electrochem. Soc. Meeting, Pittsburgh (1978).